Article

Living material assembly of bacteriogenic protocells

https://doi.org/10.1038/s41586-022-05223-w

Received: 26 October 2021

Accepted: 10 August 2022

Published online: 14 September 2022

Check for updates

Can Xu[1], Nicolas Martin[2], Mei Li[1,3] ✉ & Stephen Mann[1,3,4,5] ✉

Advancing the spontaneous bottom-up construction of artificial cells with high organizational complexity and diverse functionality remains an unresolved issue at the interface between living and non-living matter[1–4]. Here, to address this challenge, we developed a living material assembly process based on the capture and on-site processing of spatially segregated bacterial colonies within individual coacervate microdroplets for the endogenous construction of membrane-bounded, molecularly crowded, and compositionally, structurally and morphologically complex synthetic cells. The bacteriogenic protocells inherit diverse biological components, exhibit multifunctional cytomimetic properties and can be endogenously remodelled to include a spatially partitioned DNA–histone nucleus-like condensate, membranized water vacuoles and a three-dimensional network of F-actin proto-cytoskeletal filaments. The ensemble is biochemically energized by ATP production derived from implanted live *Escherichia coli* cells to produce a cellular bionic system with amoeba-like external morphology and integrated life-like properties. Our results demonstrate a bacteriogenic strategy for the bottom-up construction of functional protoliving microdevices and provide opportunities for the fabrication of new synthetic cell modules and augmented living/synthetic cell constructs with potential applications in engineered synthetic biology and biotechnology.

Establishing true-to-life functionality in synthetic cells is a global grand challenge that traverses multiple fields, including synthetic biology, bioengineering and origin of life research (see, for example, https://www.basyc.nl/; https://www.buildacell.org/; and https://www.syntheticcell.eu). The transitioning from inert capsule-based technologies to dynamical microcompartmentalized entities capable of autonomous cytomimetic behaviour requires breakthrough advances in functional integration and on-board energization of multiplexed microsystems. So far, the engineering of synthetic cellular systems (protocells) has been mainly approached using self-assembled vesicles[5–7], semi-permeable microcapsules[8–14] and membraneless or coated coacervate microdroplets[15–18]. These compartments provide a controllable medium for the encapsulation and exchange of biological and non-biological components that are experimentally selected to demonstrate single functions such as gene expression[5,8,19,20], enzyme catalysis[21] and ribozyme activity[22,23] within the synthetic cell models. Achieving high organizational and functional complexity in these constructs is methodologically demanding owing to difficulties in establishing sufficient compositional diversity and chemical complementarity by conventional methods of microcompartmentalization under close-to-equilibrium conditions. These limitations restrict the structural and chemical complexity of current protocell models, inhibit the implementation of integrated componentry and impede the development of energized cytomimetic systems.

To address these issues, here we developed an approach to engineer the first generation of energized protocells based on prokaryotes as structural and functional building blocks. In brief, we implement a living material assembly process for the bottom-up endogenous construction of membrane-bounded, molecularly crowded synthetic cells with multifunctional cytomimetic properties. Our approach is based on the co-capture and on-site processing of two spatially segregated bacterial colonies (*E. coli* and *Pseudomonas aeruginosa* (PAO1 strain)) that are co-associated with individual poly(diallyldimethylammonium chloride) (PDDA)/adenosine 5′-triphosphate (ATP) coacervate microdroplets. In situ lysis of the captured bacteria spontaneously gives rise to lipid-membrane-coated protocells enclosing an extensive repertoire of functional biological components. We demonstrate that the bacteriogenic protocells are capable of complex processing such as the endogenous production of ATP through proto-metabolic activity (glycolysis) and inherit a sufficient complement of the bacterial gene expression machinery to implement in vitro transcription and translation. To increase the level of internal structural organization, we use a combination of endogenous polynucleotide liquid–liquid phase separation, ATP-driven supramolecular protein assembly and hypotonicity to augment the synthetic cells with a spatially partitioned nucleus-like DNA–histone condensate, 3D network of F-actin proto-cytoskeletal filaments and osmotically responsive membrane-bounded water vacuoles, respectively. As a step towards self-sustainable energization, we constructed living–synthetic hybrids in which we use implanted live *E. coli* cells as surrogate mitochondria to increase and extend the endogenous production of ATP for enhancing kinase activity, glycolysis, in vitro gene expression and cytoskeletal

[1]Centre for Protolife Research and Centre for Organized Matter Chemistry, School of Chemistry, University of Bristol, Bristol, UK. [2]Univ. Bordeaux, CNRS, Centre de Recherche Paul Pascal, UMR5031, Pessac, France. [3]School of Materials Science and Engineering, Shanghai Jiao Tong University, Shanghai, P. R. China. [4]Max Planck-Bristol Centre for Minimal Biology, School of Chemistry, University of Bristol, Bristol, United Kingdom. [5]Zhangjiang Institute for Advanced Study (ZIAS), Shanghai Jiao Tong University, Shanghai, P. R. China. ✉e-mail: mei.li@bristol.ac.uk; s.mann@bristol.ac.uk

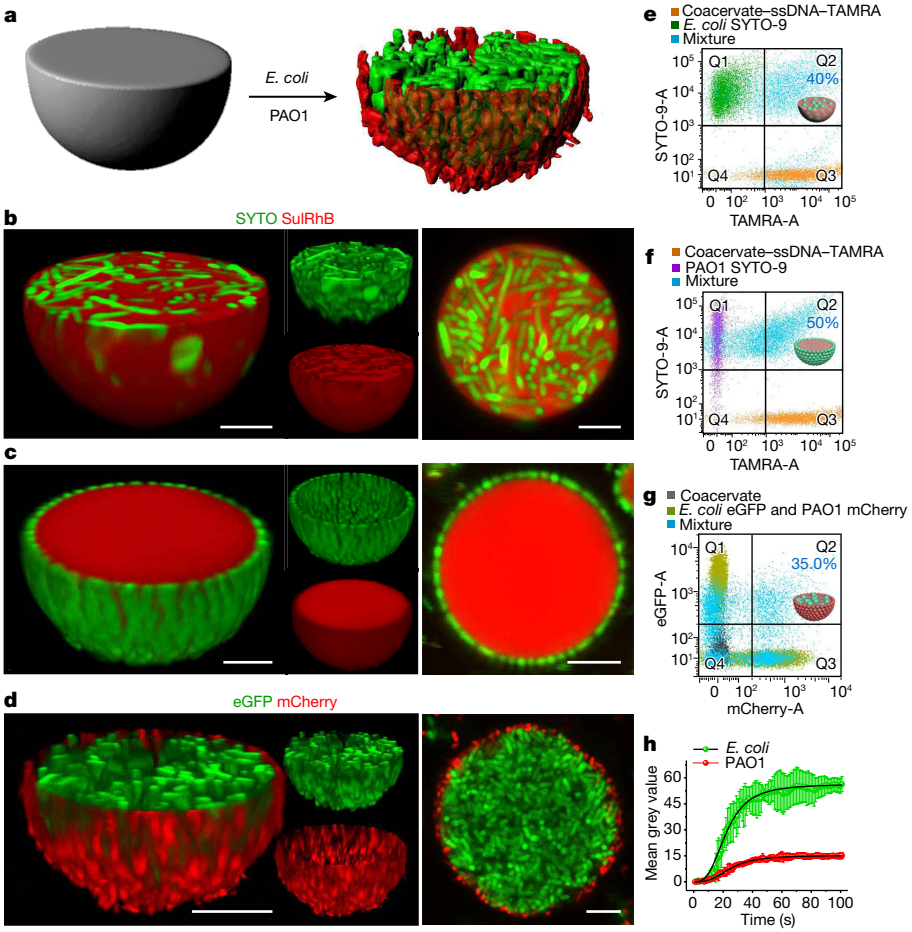

Fig. 1 | Spontaneous capture of bacterial colonies in coacervate microdroplets. a, Specific uptake of live *E. coli* (green) and surface adsorption of PAO1 (red) cells in PDDA/ATP coacervate microdroplets. **b**–**d**, Confocal microscopy images of coacervate droplets after spontaneous capture of live *E. coli* (**b**), PAO1 (**c**) and a binary population of *E. coli* and PAO1 (**d**) cells. 3D (left) and 2D (right) fluorescence images are shown, with green/red fluorescence overlays, and filtered images. The fluorescence labels in **b** and **c** show coacervate (Sul-RhB, red) and bacteria (SYTO-9, green, DNA stain). The green and red fluorescence in **d** originate from expressed eGFP and mCherry. Scale bars, 5 µm. **e**–**g**, FACS fluorescence-gated analysis of the following coacervate microdroplet–bacteria mixtures: ssDNA–TAMRA-labelled droplets (orange), free SYTO-9-stained *E. coli* (green) and droplets with captured *E. coli* SYTO-9 (blue) (**e**); ssDNA–TAMRA droplets (orange), free SYTO-9-stained PAO1 (purple) and droplets with captured PAO1 SYTO-9 (blue) (**f**); non-fluorescent microdroplets (grey), free *E. coli* eGFP and PAO1 mCherry cells (olive green) and droplets with co-captured *E. coli* eGFP and PAO1 mCherry cells (blue) (**g**). For **e** and **f**, the quadrants comprise free *E. coli* (46%, gate Q1), free droplets (12%, Q3) and droplets with captured *E. coli* bacteria (40%, Q2) (**e**), and free PAO1 (42%, Q1) , free droplets (7%, Q3) and droplets with captured PAO1 (50%, Q2) (**f**); impurities (Q4) were 2% in both cases. For **g**, the quadrants show free *E. coli* eGFP (33%, gate Q1), free PAO1 mCherry (22%, Q3), free unlabelled droplets (10%, Q4) and droplets with co-captured bacteria (35%, Q2) (**g**). Data were recorded after 5 min for a total population size of 1×10^6. **h**, Time-dependent fluorescence plots of the co-capture of *E. coli* (green) and PAO1 (red) cells in individual coacervate droplets. The curves were fitted to logistic sigmoid functions. The *E. coli* and PAO1 time midpoints ($t_{1/2}$) were 22 s and 25 s; growth-rate indices were 1.75 and 5.9; and equilibrium times (first derivative ≈ 0) were around 70 s and 80 s, respectively. $n = 4$ protocells measured. Data are mean ± s.d.

assembly within the bacteriogenic protocells. The protoliving constructs adopt an amoeba-like external morphology and decreased membrane permeability due to on-site bacterial metabolism and growth to produce a cellular bionic system with integrated life-like properties. Together, our results demonstrate a bacteriogenic strategy for the bottom-up construction of functional protocellular microdevices and provide opportunities for the fabrication of synthetic cell modules and augmented living/synthetic cell constructs with potential applications in engineered synthetic biology and biotechnology.

Assembly of bacteriogenic protocells

To implement the endogenous assembly of bacteriogenic protocells, we first constructed a microscale building site comprising 5–30-µm-diameter pre-former PDDA/ATP coacervate droplets of spatially segregated live bacterial cells (Fig. 1a). Single populations of *E. coli* cells were sequestered at high concentrations into the interior of the membrane-free coacervate droplets within a few minutes to produce viable microcompartmentalized colonies (Fig. 1b and Supplementary Video 1). By contrast, PAO1 cells were almost instantaneously adsorbed onto the droplet surface to produce a shell of living bacteria (Fig. 1c and Supplementary Video 2). Importantly, the addition of a mixture of *E. coli* and PAO1 cells gave rise within a few minutes to single coacervate droplets comprising an internally segregated *E. coli* population surrounded by a thin continuous shell of PAO1 cells (Fig. 1d and Supplementary Video 3). Measurements of the size distributions of the coacervate droplets showed that minimal changes occurred for the capture of *E. coli* cells, indicating that sequestration of the bacteria within the droplets did not change the stability of the coacervate phase (Extended Data Fig. 1a–d). However, capture of PAO1 cells specifically at the droplet interface inhibited droplet fusion such that the protocell population was more monodisperse (Extended Data Fig. 1e,f).

A similar decrease in polydispersity was also observed when both *E. coli* and PAO1 cells were co-captured by the PDDA/ATP coacervate droplets (Extended Data Fig. 1g,h).

Quantitative fluorescence-activated cell sorting (FACS) analysis of mixed suspensions of coacervate droplets and *E. coli* or PAO1 cells confirmed that the bacteria were captured at relatively high efficiency (typically 40–50%) after 5 min of incubation (Fig. 1e,f). Similar experiments on droplets containing captured *E. coli* and PAO1 cells with expressed eGFP or mCherry fluorescence, respectively, indicated that the co-loading efficiency was around 35% (Fig. 1g). Corresponding time-dependent fluorescence measurements of single coacervate droplets showed logistic growth rates in eGFP and mCherry fluorescence intensities up to threshold values as the droplet interior became filled with bacteria and the assembly of the bacterial shell was completed (Fig. 1h). Staining of the captured bacteria and time-dependent FACS analyses indicated that the majority of the cells (73%) survived for at least 24 h after the addition to the coacervate droplets (Extended Data Fig. 1i–o). The coacervate-containing bacterial cells could be physically manipulated without disintegration (Extended Data Fig. 1p,q) and remained genetically active within the coacervate matrix (Extended Data Fig. 1r,s).

Having assembled the stable living pre-former droplets, we used on-site processing to reconfigure and repurpose the spatially segregated bacterial colonies into membrane-bounded, molecularly crowded protocells with complex microstructures and diverse bioderived functionalities (Fig. 2a). To achieve this, we implemented the stepwise in situ lysis of the co-captured bacteria populations using a cell wall hydrolase (lysozyme) and antimicrobial peptide (melittin)[24] to release an extensive suite of bacterial membrane lipids/proteins and cytoplasmic components into the adjacent coacervate milieu (Extended Data Fig. 2a and Supplementary Figs. 1 and 2). Short lysis times (0.5 h) generated coacervate droplets containing a living *E. coli* colony bounded by a 300–500-nm-thick shell of PAO1-derived membrane constituents (Fig. 2b). Extending the processing time so that lysis of both types of bacteria occurred gave rise to structurally and compositionally complex protocells that consisted of a spatially segregated membrane of PAO1 lipids, which enclosed a coacervate matrix consisting principally of incarcerated *E. coli* cytoplasmic components along with PAO1-membranized water vacuoles (Fig. 2c–e, Extended Data Fig. 2b–g and Supplementary Fig. 3). Although proteins and polynucleotides did not readily leach from the protocells owing to their strong affinity with the coacervate matrix (Fig. 2c,d), the PAO1-derived membrane was permeable to small-molecule fluorescent dyes as well as macromolecular solutes, which could be readily taken up from the external solution (Supplementary Fig. 4). The high membrane permeability was consistent with scanning electron microscopy images of freeze-dried bacteriogenic protocells, which showed a disordered arrangement of cytomembrane fragments on the surface of the droplets (Extended Data Fig. 2h,i). FACS quantitative analysis of samples prepared from co-captured *E. coli* and PAO1 cells with expressed eGFP and mCherry fluorescence, respectively, indicated that the percentage of bacteriogenic protocells produced after lysis was about 30% (Supplementary Fig. 5).

Quantitative component analyses indicated that the bacteriogenic synthetic cells inherited protein, lipid, RNA and DNA contents of 16, 3, 3 and 1 wt%, respectively (Fig. 2f). Full protein typing was achieved by liquid chromatography–mass spectrometry (LC–MS) proteomics, which indicated that approximately 83% (2,237 proteins) of the combined library of bacterial proteins were retained by the protocells (Fig. 2g). Most (65%) of the retained proteins from the two populations were derived from the *E. coli* cells initially housed within the interior of the droplets. Of these, 97% of the *E. coli* protein types were associated with the protocells compared with 65% of those in the PAO1 proteome (Fig. 2g). In terms of molecular function, proteins with catalytic (43%), binding (32%) and structural (14%) roles were highly represented, whereas anatomical (48%) and intracellular entities (40%) along with protein-containing complexes (12%) were dominant as cellular components. These proteins were primarily associated with cellular (44%) and metabolic processes (40%), with the remaining proteins assigned principally to biological regulation, localization and sensing (Fig. 2h).

Cytomimetic properties

Given the extensive repertoire of biological components embodied within the bacteriogenic protocells, we sought to exploit the compositional complexity for the fabrication of synthetic cell modules with diverse cytomimetic properties operating at the level of individual enzymes, proto-metabolic pathways (glycolysis) and information networks (in vitro gene expression).

Retention of functional enzymes within the ensemble of released components was demonstrated by monitoring the activity of alkaline phosphatase, protease, lipase and β-galactosidase (β-gal) within the bacteriogenic protocells after exposure to appropriate fluorogenic small-molecule substrates in the external environment. In each case, production of the fluorescent outputs occurred homogeneously throughout the interior of the bacterially derived protocells and the products retained predominantly within the coacervate matrix (Fig. 3a–f, Supplementary Video 4, Extended Data Fig. 3a–d and Supplementary Fig. 6). We also tested whether the bacteriogenic protocells inherited a sufficient complement of coordinated enzymes to implement the ten-enzyme cascade required for glycolysis[25]. For this, we added glucose-containing Luria–Bertani (LB) broth to protocells containing lactate dehydrogenase and assayed the onset of proto-metabolic activity through the conversion of pyruvate to L-lactate along with formation of the reduced purple dye (formazan). Time-dependent spectroscopy measurements showed significant glycolysis activity in the protocell population (Fig. 3g,h), along with a blue-purple colouration and formation of insoluble formazan within the protocell interior (Fig. 3i,j and Extended Data Fig. 3e), indicating that sufficient levels of bacterially derived cell respiration components were released by lysis and retained within the cytoplasmic-like coacervate matrix.

As bacterial lysates can be used for in vitro translation and transcription[26], we loaded selected components of an expression system (buffer, T7 promoters and polymerases, amino acids, nucleotides and tRNA) and a plasmid (pEXP5-NT/deGFP) for deGFP expression into PDDA/ATP coacervate droplets. Notably, the bacterial lysate accompanying the cell-free expression kit was not included. We next used the primed droplets to capture *E. coli* and PAO1 cells followed by in situ lysis, bacteriogenic protocell construction and storage on ice. As a consequence, subsequent endogenous processing of the incorporated plasmid by the protocells was dependent on inheriting a sufficient complement of gene expression machinery (such as peptidyl transferase, RNA synthetases, energy generation, translation factors (IF1, IF2, IF3) and ribosomal proteins) from in situ lysis of the bacterial cells. Gene expression was initiated by raising the temperature to 37 °C with additional feed buffer added after 30 min to sustain the system. Production of deGFP occurred specifically within the bacteriogenic protocells over 5 h to give a protein yield of 0.01 μM with maximum and minimum expression rates at 0.5 h and 3 h, respectively (Fig. 3k–m). By contrast, negligible green fluorescence was observed for synthetic cells lacking the pEXP5-NT/deGFP plasmid (Fig. 3m) or for supernatants depleted of bacteriogenic protocells (Supplementary Fig. 7). Gel electrophoresis of the extracted proteins showed a band at 27 kDa that was absent without the plasmid (Fig. 3n and Supplementary Fig. 8a), and western blotting images indicated that the 27 kDa band was stained by anti-GFP antibodies (Fig. 3o and Supplementary Fig. 8b), confirming deGFP expression within the bacteriogenic protocells.

Augmentation and remodelling

Bacterially derived synthetic cells containing both a spatially partitioned nucleus-like organelle and 3D structural network of protocytoskeletal filaments were prepared by endogenous remodelling

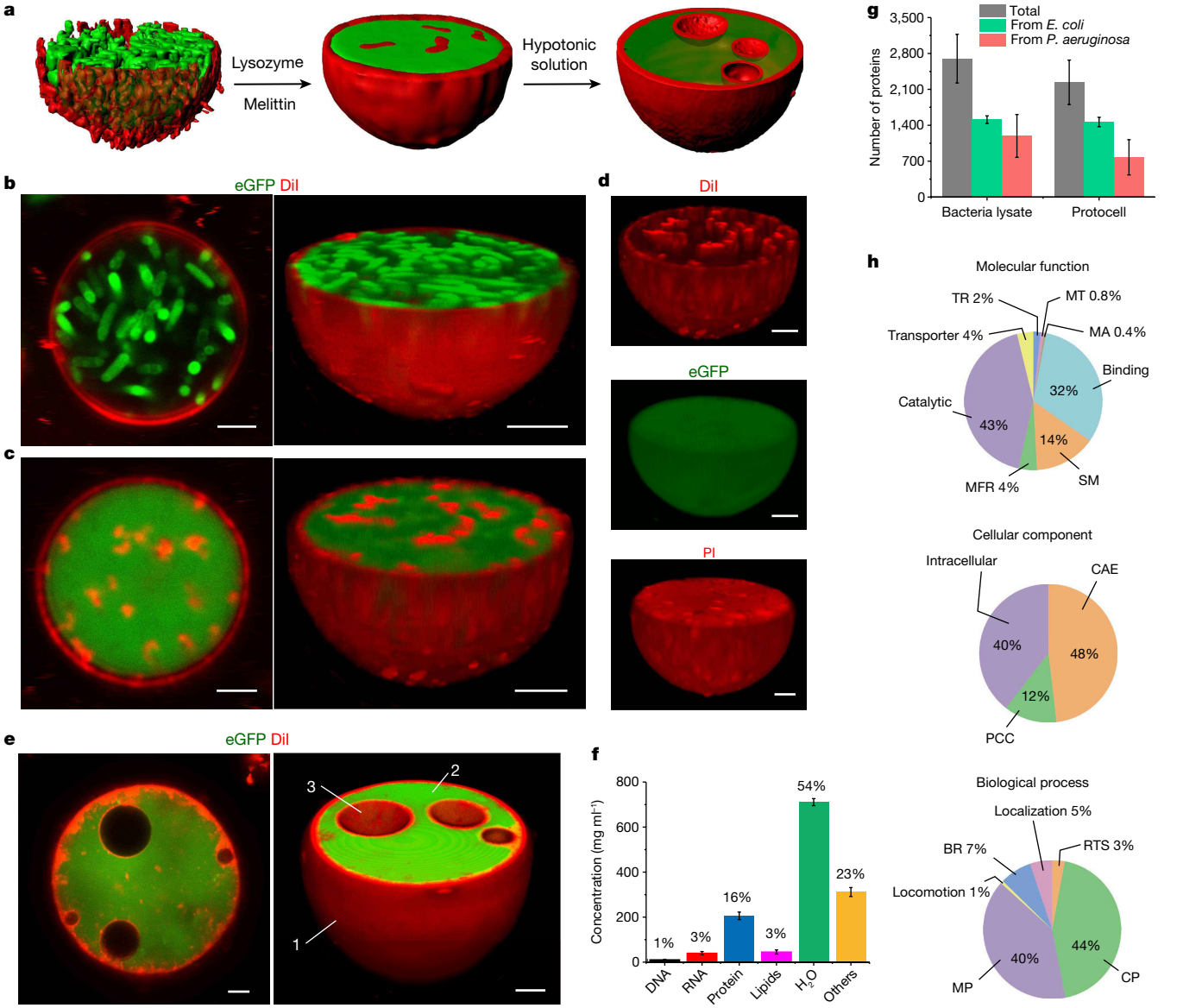

Fig. 2 | Construction of bacteriogenic protocells. a, On-site bioprocessing of living pre-former coacervate droplets into bacteriogenic protocells comprising encapsulated *E. coli*-derived cytoplasmic components (green) surrounded by a continuous PAO1-derived membrane (red) (left and middle). Right, exposure to hypotonic conditions results in water vacuole formation within the protocells. **b**,**c**, 2D and 3D green/red-overlaid confocal fluorescence microscopy images of single PDDA/ATP coacervate droplets containing spatially separated populations of living *E. coli* eGFP (green fluorescence) and lysed PAO1 cells (red fluorescence, DiI C18 stain, lipid fragments) (**b**), and after lysis of both bacteria to produce a bacteriogenic protocell (**c**). The fluorescence labels show *E. coli*-derived eGFP (green) within the protocell interior and a continuous membrane of PAO1-derived lipids (red) at the protocell surface. **d**, Corresponding filtered 3D images; cytomembrane fragments are also present within the protocell (top) along with homogeneous distributions of *E. coli*-derived eGFP (middle) and DNA (bottom; PI-red fluorescence). **e**, 2D (left) and 3D (right) confocal fluorescence microscopy images of an individual bacteriogenic protocell containing membrane-coated water-filled vacuoles (non-fluorescent region). The proto-cytomembrane (1), proto-cytoplasm (2) and water-filled vacuole (3) are shown. Staining was performed as described in **c**. For **b**–**e**, scale bars, 5 µm. **f**, Quantitative component analyses of bacteriogenic protocells derived from lysed mixed populations of *E. coli* and PAO1 cells. **g**, LC–MS proteomic analyses of samples of bacteriogenic protocells and a binary population of *E. coli* and PAO1 cells (no coacervate droplets). For **f** and **g**, $n = 3$ experiments. Data are mean ± s.d. Contaminating proteins/peptides such as lysozyme and melittin were excluded from the analysis. **h**, Gene Ontology term annotation and functional classification for identified proteins associated with bacteriogenic protocells. The proteins were identified in multiple subcategories (molecular functions (top), cellular components (middle) and biological processes (bottom)). BR, biological regulation; CAE, cellular anatomical entity; CP, cellular process; MA, molecular adapter; MFR, molecular function regulator; MP, metabolic process; MT, molecular transducer; PCC, protein-containing complex; RTS, response to stimulus; SM, structural molecule; TR, translation regulator.

of the cytoplasmic-like interior (Fig. 4a). Spontaneous aqueous two-phase liquid–liquid separation of a single bacterial DNA–histone condensate within the bacteriogenic protocells was achieved within the cytoplasmic-like interior by uptake of carboxymethyldextran (CM-dextran; 70 kDa). The procedure, which was dependent on the presence of linear double-stranded DNA (dsDNA) and was initially developed using native PDDA/ATP droplets (Extended Data Fig. 4a–g), involved loading the coacervate droplets with a histone protein (type II-A) and a mixture of DNase I and $MnCl_2$—the latter mixture was used to cleave the native bacterial plasmid DNA into linear fragments. This was followed by capture of a mixed population of *E. coli*/PAO1 cells and release of the bacterial plasmid DNA (and other cytoplasmic components) by lysis to

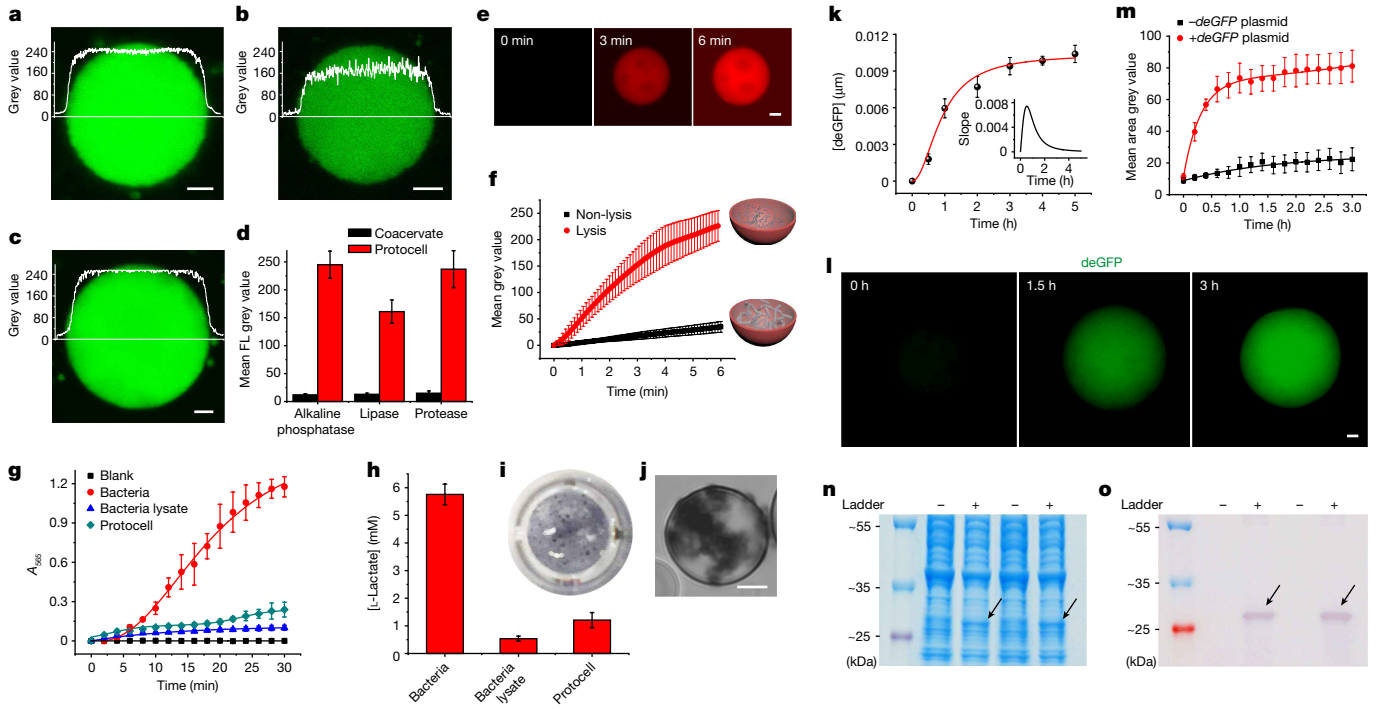

Fig. 3 | Cytomimetic properties of bacteriogenic protocells. a–**c**, Confocal fluorescence microscopy images of single protocells containing bacterially derived alkaline phosphatase (**a**), lipase (**b**) or protease (**c**) recorded 30 min after exposure to cognate enzyme substrates showing intraprotocell production or sequestration of fluorescein (**a**) or BODIPY FL dye (**b** and **c**). **d**, The mean grey values for reactions shown in **a**–**c** and for the coacervate droplet controls. **e**, Time-dependent images of a single protocell after addition of resorufin-β-D-galactopyranoside (RBG), showing endogenous β-gal-mediated production of resorufin (red fluorescence). **f**, The mean grey values with time for resorufin formation in single bacteriogenic protocells (red) or single coacervate droplets with co-captured non-lysed bacteria (black) after addition of RBG. $n = 3$. **g**, Formazan production (absorption at 565 nm (A_{565})) for native coacervate droplets (black), bacterial lysate (no droplets, blue), bacteriogenic protocells (green), and live *E. coli* and PAO1 cells (red). $n = 3$. **h**, The final concentrations of L-lactate for the experiments shown in **g**; $n = 3$. **i**, A sample well containing formazan-containing protocells (purple dots) after glycolysis. **j**, A single bacteriogenic protocell 0.5 h after glycolysis with formazan in the interior. **k**, The time-dependent increase in deGFP concentration in bacteriogenic protocells undergoing endogenous in vitro gene expression. Curve is fitted to a Hill function ($t_{1/2} = 0.9$ h, Hill coefficient = 2). Maximum expression rate is observed at 0.5 h (inset). $n = 2$. **l**, The time-dependent increase in expressed deGFP (green fluorescence) within a bacteriogenic protocell. $n = 3$. **m**, The corresponding time-dependent mean grey values for single protocells with (red) or without (black) the plasmid pEXP5-NT/deGFP. **n**,**o**, Gel electrophoresis profiles (**n**) and western blotting images (**o**) of extracted proteins after disassembly of protocells with (+) or without (–) the plasmid pEXP5-NT/deGFP. The arrows show an additional plasmid-dependent band at 27 kDa, which was stained by anti-GFP antibodies. Gel source data are provided in Supplementary Fig. 8. For **a**–**c**, **e**, **j** and **l**, scale bars, 5 μm. For **f**–**h**, **k** and **m**, data are mean ± s.d.

generate a homogeneous distribution of a linear DNA–histone complex within the protocell interior. Subsequent addition of CM-dextran and diffusion of the polysaccharide through the outer PAO1-derived membrane resulted in the nucleation of a single membrane-free DNA–histone condensate inside the individual protocells within a few tens of seconds (Fig. 4b,c). Almost all of the released bacterial DNA (99%) was confined to the nucleus-like condensate, while most (75%) of the released bacterial proteins were sequestered into the molecularly crowded cytoplasmic-like region of the protocells (Fig. 4d,e). Similar experiments involving bacterially derived protocells without preloaded DNase I and $MnCl_2$ resulted in the nucleation of large numbers of small (0.3–2 μm) plasmid DNA–histone condensates throughout the CM-dextran-enriched phase (Fig. 4f and Extended Data Fig. 4h,i). When exposed to hypotonic conditions, the remodelled protocells were further elaborated with membrane-coated water vacuoles to produce synthetic cells that exhibited multiple types of spatially segregated cytomimetic structures (Fig. 4g,h).

Having established a protocol for the in situ condensation and spatial localization of bacterial DNA within the protocells, we sought to restructure the molecularly crowded proto-cytoplasmic region by on-site energy-driven supramolecular assembly of a F-actin cytoskeletal-like filamentous network to produce a self-supported cytomimetic model[27]. Initial experiments using PDDA/ATP pre-former coacervate droplets indicated that G-actin and Mg^{2+} ions were readily taken up by the bacteriogenic protocells and that in situ F-actin assembly was activated endogenously by the coacervate-derived ATP (Extended Data Fig. 5a). However, as only short filaments of F-actin were produced owing to the high native ATP concentration (around 200 mM)[28], we prepared the subcompartmentalized bacteriogenic protocells using PDDA/uridine-5′-triphosphate (UTP) coacervate droplets (Extended Data Fig. 5b–d) and preloaded the droplets with an enzyme-based ATP-generating system based on pyruvate kinase (PK), phosphoenolpyruvate (PEP) and ADP[29] (Fig. 4i). Subsequent uptake of G-actin and Mg^{2+} initiated F-actin assembly specifically within the synthetic cells and transformed the bacteriogenic constructs into hydrogelled microstructures with retention of the spherical morphology (Fig. 4j). The results indicated that the on-board generation of ATP arising from the encapsulated PK–PEP–ADP cascade over a period of approximately 20 min was sufficient to produce the controlled restructuring of the protocell interior. This was confirmed by confocal fluorescence microscopy images of single protocells, which showed the presence of a localized low-density network of F-actin microfilaments specifically dispersed within the proto-cytoplasmic region but not in the phase-separated DNA–histone subcompartment (Fig. 4k–m and Extended Data Fig. 5e).

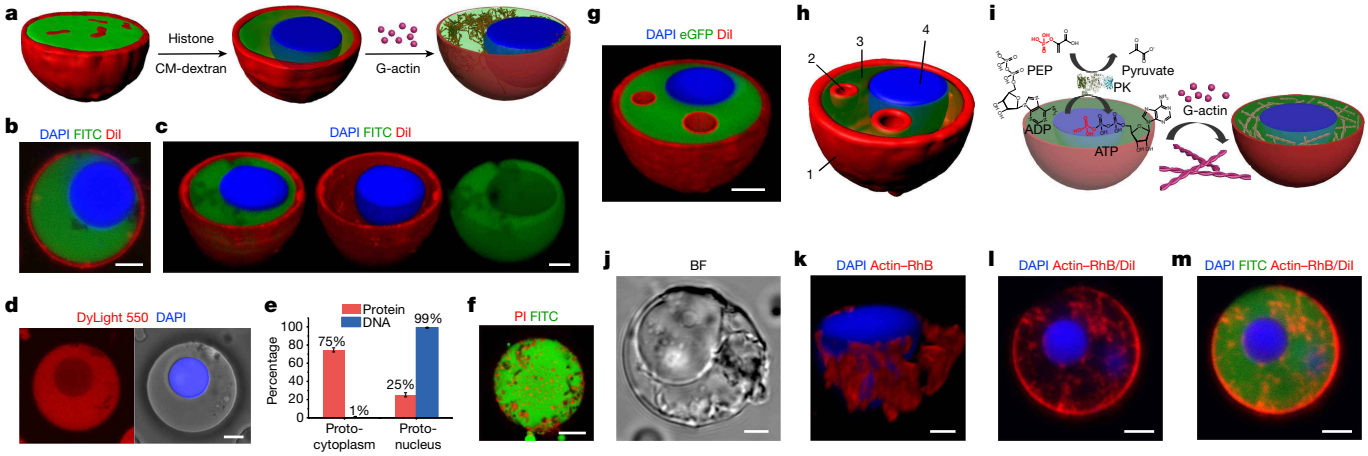

Fig. 4 | On-site augmentation of bacteriogenic protocells. a, Bacteriogenic protocells (left, outer membrane (red), proto-cytoplasm (green)) are structurally remodelled by endogenous DNA–histone liquid–liquid phase separation (centre) and ATP-driven assembly of GTP (right) to produce a single bacterial DNA–histone proto-nucleus (blue) and a 3D network of proto-cytoskeletal filaments (brown). **b**, Fluorescence microscopy image of a single bacteriogenic protocell containing histone, DNase I and $MnCl_2$ recorded 20 min after addition of FITC–CM-dextran. Blue, DNA–histone condensate; green, CM-dextran-enriched proto-cytoplasm; red, PAO1-derived lipids. **c**, Red/green/blue (left), red/blue (middle) and green (right) filtered 3D images of the protocell displayed in **b** showing spatially segregated cytomimetic structures. **d**, Images showing partial exclusion of bacterial proteins (red) from the DNA–histone condensate (blue). **e**, The percentage of protein and DNA in the cytoplasmic- and proto-nucleus-like regions of bacteriogenic protocells. $n = 3$. For **e**, data are mean ± s.d. **f**, A single bacteriogenic protocell prepared as described in **b** but in the absence of DNase I and $MnCl_2$; multiple DNA–histone condensates (red) are distributed in the proto-cytoplasm (green). **g**,**h**, Fluorescence microscopy (**g**) and 3D reconstruction (**h**) images of a bacteriogenic protocell under hypotonic conditions. The proto-cytomembrane (1), water-filled vacuole (2), proto-cytoplasm (including CM-dextran) (3) and proto-nucleus (4) are shown. Staining was performed as described in **b**, except green fluorescence was from expressed eGFP. **i**, F-actin assembly in PDDA/UTP-based bacteriogenic protocells charged with PK, PEP and ADP. PK transfers phosphate from PEP to ADP to yield pyruvate and ATP. G-actin and Mg^{2+} uptake results in ATP-driven polymerization and microfilament assembly only in the proto-cytoplasm. **j**,**k**, Bright-field image (**j**) and the corresponding 3D fluorescence image (**k**) of a single bacteriogenic protocell prepared as described in **i**. Red, F-actin network; blue, DNA–histone proto-nucleus. **l**,**m**, Images of a single bacteriogenic protocell showing the proto-cytoskeletal network (red), membrane-free DNA–histone condensate (blue) and PAO1-derived outer membrane (red) (**l**); the proto-cytoplasm (green) is also imaged in **m**. For **b**–**d**, **f**, **g** and **j**–**m**, scale bars, 5 µm.

Live cell/synthetic cell constructs

Given the potential for compositional, structural and functional complexity in the bacteriogenic protocells, we sought to couple these attributes to an internal ATP-based energy source as a step to increasing the autonomy and self-sufficiency of the life-like constructs. To achieve this, we implanted *E. coli* cells into PDDA/UTP-based bacteriogenic protocells (Fig. 5a), and used the incarcerated living cells as surrogate mitochondria for the endogenous production of ATP[30]. Confocal fluorescence microscopy images indicated that the *E. coli* cells were sequestered specifically into the cytoplasmic-like space; by contrast, no cells were observed in the DNA–histone-enriched proto-nucleus (Fig. 5b). Typically, 10–50 bacteria were initially captured within the cellular bionic system. Live/dead staining of the constructs indicated that many of the implanted *E. coli* cells remained viable after entrapment for 3 h (Extended Data Fig. 6a). Corresponding time-dependent FACS data indicated that the population of *E. coli* cells increased by approximately 10 times over a period of 48 h with the percentage of live cells decreasing from 98% (1 h) to 60% (48 h) (Fig. 5c,d and Extended Data Fig. 6b–d). Growth of the trapped bacterial colony produced a threefold increase in the total protein concentration within the protocells over a period of 48 h (Fig. 5e).

To energize the living/synthetic cell construct, we initiated ATP production in the incarcerated *E. coli* cells by addition of glucose (in LB broth) and took advantage of the extracellular secretion of the energy-rich mononucleotide[31] to chemically charge the co-located bacteriogenic protocells (Supplementary Fig. 9). As a consequence, continuous biologically mediated ATP production in the PDDA/UTP-based bacteriogenic protocells was sustained for up to 36 h compared with 20 min in the presence of a sequestered PK–PEP–ADP enzyme-based pathway (Fig. 5f). Bioproduction of ATP was fitted to an exponential decay curve that attained equilibrium after around 36 h with a maximum ATP concentration of 1.65 mM under the conditions typically used (Extended Data Fig. 7a). Importantly, ATP biogeneration within the hybrid protocells was readily sustained by replenishing the nutrients in the external medium, whereas the addition of new substrates (ADP, PEP) to the enzyme-based pathway disrupted the structural integrity of the protocells.

Biogeneration and extracellular secretion of ATP resulted in prolonged enzyme activity and gene expression, as well as increased levels of F-actin polymerization in the living/synthetic constructs. For example, kinase activity was approximately doubled compared with PDDA/UTP bacteriogenic protocells containing released bacterial lysate (no live *E. coli* cells) and increased 1.3-fold in comparison to the implanted PK–PEP–ADP pathway (no live *E. coli* cells) (Fig. 5g and Extended Data Fig. 7b–d). In vitro gene expression of *deGFP* was extended from 3 h to 24 h with a final deGFP concentration of around 0.015 µM (Fig. 5h,I and Extended Data Fig. 7e–j) and pyruvate production was increased 1.7-fold due to sustained glycolysis in the implanted bacteria (Extended Data Fig. 7k). On-site assembly of F-actin after passive uptake of G-actin and Mg^{2+} ions gave rise to an extensive network of protein filaments that filled most of the proto-cytoplasmic space within 30 min (Fig. 5j,k and Extended Data Fig. 8a–c). As a consequence, living bacteria, a single DNA–histone subcompartment and water vacuoles were immobilized in a cytoskeletal-like framework to produce a self-supporting cellular bionic system that remained structurally intact in water and salt solutions for at least 7 days (Fig. 5l and Extended Data Fig. 8d). By contrast, living/synthetic constructs prepared without F-actin were stable for only up to 3 days in buffer and disassembled immediately under hypertonic conditions (Extended Data Fig. 8e).

Finally, we sought to take advantage of the continuous biogeneration of metabolic products within the bacteriogenic protocells to implement changes in membrane interfacial tension as a step towards producing living/synthetic cell hybrids with non-spherical

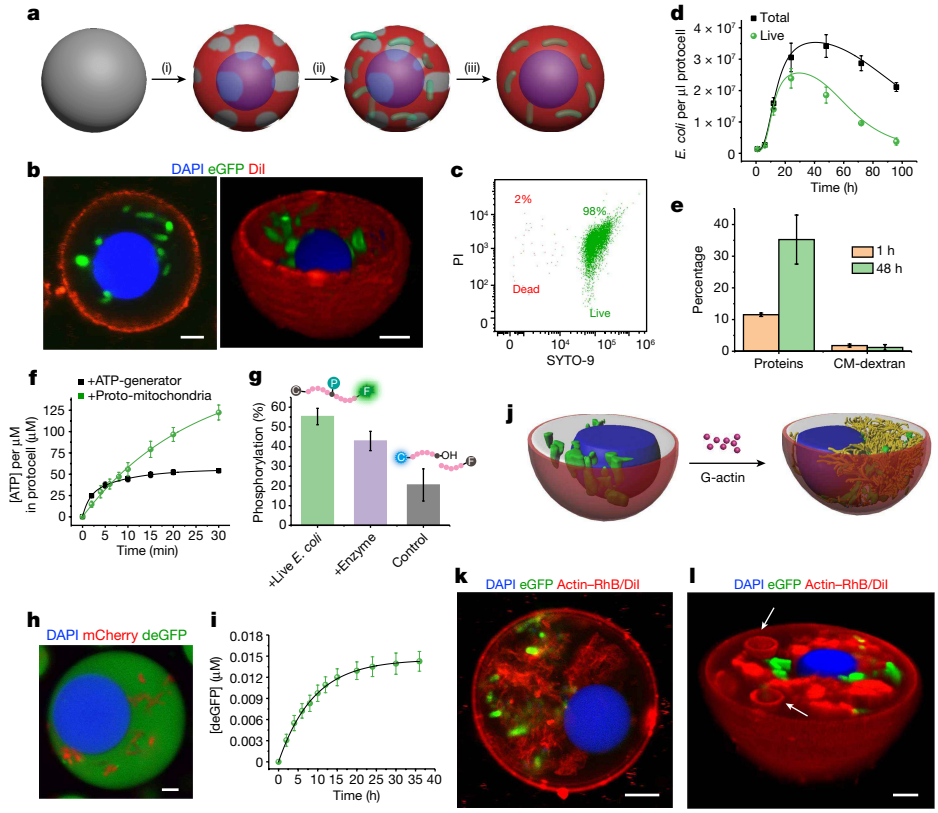

Fig. 5 | Live-cell energization of bacteriogenic protocells. a, Implantation of live *E. coli* cells in bacteriogenic protocells. Construction of PDDA/UTP-based bacteriogenic protocells with a DNA–histone subcompartment and incomplete PAO1-derived membrane (i). Penetration of living *E. coli* and capture within the proto-cytoplasmic region (ii). Addition of PAO1-derived lipids and sealing of the protocell membrane (iii). **b**, 2D (left) and 3D (right) fluorescence images showing *E. coli* eGFP cells (green) in the proto-cytoplasmic regions of a single bacteriogenic protocell after membrane resealing (red). Blue, DNA–histone condensate. **c**, FACS live/dead analysis of bacteriogenic protocells containing SYTO-9/PI-stained *E. coli* cells. **d**, Time-dependent plots of the mean numbers of *E. coli* cells (total, black; live, green). **e**, Protein and CM-dextran levels in bacteriogenic protocells after incubation for 1 h (orange) and 48 h (green). **f**, Time-dependent plots of ATP concentration in bacteriogenic protocells by entrapped live *E. coli* cells (proto-mitochondria, green) or ATP-generation (PK–PEP–ADP pathway, black). **g**, Kinase activity in bacteriogenic protocells with entrapped live *E. coli* cells (green, 55%), encapsulated PK–PEP–ADP pathway (purple, 43%) or ATP control (bacterial lysate, grey column, 21%). **h**, In vitro gene expression of *deGFP* (green) in the proto-cytoplasmic region of a single hybrid protocell. Blue, DNA–histone subcompartment; red, entrapped live *E. coli* cells. **i**, deGFP expression over 40 h for a population of hybrid protocells. The exponential decay curve is shown ($[deGFP]_{max}$ = 0.015 µM, $t_{1/2}$ = 9 h). **j**, F-actin assembly in bacteriogenic protocells containing ATP-generating live *E. coli* cells (green) and a DNA–histone proto-nucleus (blue). **k**, 2D image of a living/synthetic cell construct with F-actin microfilament network (red), DNA–histone subcompartment (blue) and guest *E. coli* eGFP cells (green). **l**, 3D image of a hybrid protocell exposed to hypotonic conditions for 30 min; membrane-coated water vacuoles (arrows) are trapped within the remodelled proto-cytoplasm. For **b**, **h**, **k** and **l**, scale bars, 5 µm. n = 3. For **d**–**g** and **i**, data are mean ± s.d.

morphology. In the absence of incarcerated *E. coli* cultures, mounting the F-actin-containing spherical bacteriogenic protocells onto pegylated glass substrates and leaving the samples at room temperature in LB broth for 48 h resulted in minimal changes in structure and morphology (Extended Data Fig. 9a). By contrast, similar experiments with bacteriogenic protocells containing encapsulated live *E. coli* cells and a F-actin network gave rise to progressive changes in morphology (Fig. 6a). Within 48 h, most of the spherical microstructures adopted a more irregular cell-like form while maintaining their outer membrane structure and complex internal organization (Fig. 6b), suggesting that the proto-cytoskeletal filaments were structurally dynamic over extended time scales. During this period, the average number of *E. coli* cells per protocell increased by approximately eightfold within the first 24 h, after which the entrapped population of live cells decreased by approximately 35% after 48 h (Fig. 6c). Growth of the bacteria was associated with a twofold increase in the average protocell volume over 48 h (Fig. 6d) and progressive decreases in UTP concentration (Supplementary Fig. 10), possibly due to bacterial consumption of the nucleotide.

Given that the amoeba-like morphology was also observed after 24–48 h for living cell/protocell constructs prepared without a F-actin network (Extended Data Fig. 9b,c), we ruled out the possibility that the changes in form were associated with anisotropic mechanical forces induced by ATP-mediated formation of the cytoskeletal-like matrix. Moreover, other studies showed that, although time-dependent increases in bulk wettability were observed for single droplets of concentrated suspensions of the living/synthetic hybrids mounted onto pegylated glass slides (Extended Data Fig. 9d,e), mounting the same constructs onto hydrophobic plastic or non-modified glass surfaces also showed amoeba-like morphologies after 48 h incubation, indicating that specific interactions with the substrate were not critical in determining the shape change (Extended Data Fig. 9f). Indeed, low-resolution confocal microscopy images of the living/synthetic constructs recorded in aqueous suspension also showed the non-spherical morphology (Extended Data Fig. 9g). We therefore concluded that an endogenous mechanism associated with prolonged activity of the entrapped *E. coli* cells was most likely responsible for the morphological changes. In this regard, no changes in shape were

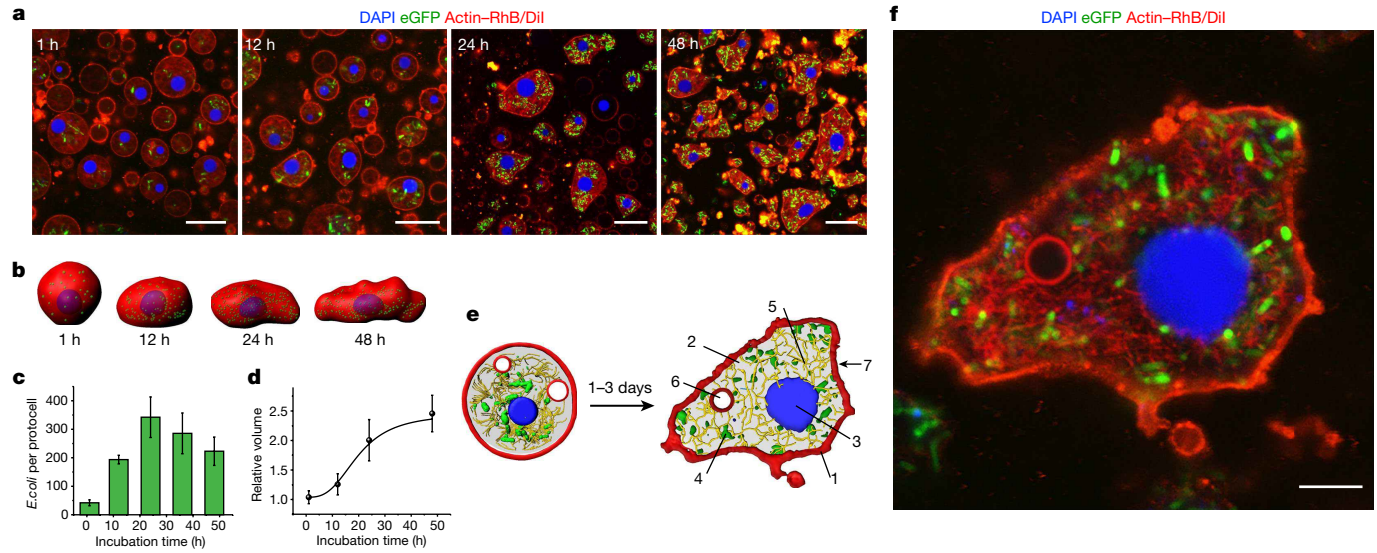

Fig. 6 | Live-cell-mediated morphogenesis in bacteriogenic protocells. **a**, Time series of confocal fluorescence microscopy images of spherical bacteriogenic protocells with entrapped *E. coli* eGFP cells and F-actin (1 h) showing progressive transformation (12–48 h) into amoeba-like living/synthetic constructs due to on-site *E. coli* activity. Data were recorded at given time intervals from different populations. Red, F-actin and outer membrane; blue, DNA–histone condensate; green, guest live *E. coli* cells. **b**, Corresponding time series of 3D reconstruction images. The colours are as described in **a**. **c**, Time-dependent changes in the numbers of live *E. coli* cells per protocell. $n = 3$. Data are mean ± s.d. **d**, Time-dependent plot of relative volumes for single living/synthetic constructs. $n = 3$. Data are mean ± s.d. **e**,**f**, Diagram (**e**) and corresponding 2D confocal fluorescence microscopy image (**f**) of the functional protoliving synthetic cell with seven cytomimetic features: outer membrane (1); molecularly crowded proto-cytoplasm (2); membrane-free DNA–histone proto-nucleus (3);surrogate mitochondria (*E. coli* cells) (4); proto-cytoskeleton (5); membrane-bounded spherical water vacuoles (6); and amoeba-like cell morphology (7). For **a** and **f**, scale bars, 10 µm.

observed after short periods (1 h) when the bacteriogenic protocells were loaded with extremely high loadings of freshly washed *E. coli* cells (Extended Data Fig. 9h), suggesting that extended metabolic activity of the incarcerated bacterial cells, rather than an increase per se in the population density within the protocells, was responsible for the transition to the amoeba-like form. For example, over a period of 30 h, the PDDA:UTP:CM-dextran:protein:DNA concentration ratio changed from 1:1:0.5:2:0.03 to 1:0.6:0.5:4.7:0.07, indicating that the formation of the irregular cell-like form was associated with a considerable depletion of UTP along with a marked increase in bacterially derived proteins. It seems feasible that the latter were responsible for lowering the membrane interfacial tension, resulting in the loss of the spherical morphology.

Interestingly, the permeability of the outer membrane to macromolecular diffusion decreased markedly with change in shape such that dextran above a molecular mass of 10 kDa, BSA–FITC (66 kDa), eGFP (32 kDa) and single-stranded DNA (8 kDa) were no longer taken up into living/synthetic hybrids that were biologically active for more than 20 h (Extended Data Fig. 10a–f). On the basis of these observations, we speculate that the continuous production of bacterial lipids facilitated partially sealing of defects in the outer membrane, as well as increasing membrane surface area and elasticity.

Discussion

An ensemble of cytomimetic features was integrated into a synthetic cell construction pathway using a living material assembly process in which prokaryotes are used as on-site repositories of key structural and functional building units. Depending on the extent of the construction process, a total of seven distinct cytomimetic attributes can be integrated into the bacteriogenic protocells (Fig. 6e,f). Implementation of the basic processing strategy gives rise to complex synthetic cells with a bacterially derived semipermeable outer membrane and internal molecularly crowded proto-cytoplasm containing a PDDA/ATP (UTP) coacervate, an extensive suite of bacterial proteins and polynucleotides, a functional metabolic network, and intact translation and transcription machinery. Further elaboration of the synthetic cells can be achieved endogenously by structural augmentation with a single membrane-free DNA–histone nucleus-like condensate, osmotically responsive membrane-bounded water vacuoles[32,33] and a primitive F-actin cytoskeletal-like network. In each case, the additional design features are implemented without compromising the multiple cytomimetic functions. Higher-level operations are introduced by using implanted live *E. coli* cells as surrogate mitochondria for energization, which prolongs ATP bioproduction and transforms the spherical bacteriogenic protocells into a cellular bionic system with amoeba-like cell morphology.

Our living-material assembly approach provides opportunities for the bottom-up construction of highly integrated synthetic cells and augmented living/synthetic cell constructs. A critical aspect of the construction sequence is the spontaneous coacervate droplet-mediated capture and spatial segregation of *E. coli* and PAO1 cells that together enable on-site processing and retention of diverse bacterial components for synthetic cell elaboration. Thus, using this strategy, it should be possible to not only establish artificial organelles based on lysosomes, peroxisomes and storage granules within the bacteriogenic protocells, but also reconfigure the spatial organization of the bacterially derived components. For example, the spatial distribution of live *E. coli* and PAO1 cells in the initial pre-former coacervate droplets can be modulated by changes in the coacervate composition (Supplementary Fig. 11). In the longer term, the possibility of spatially coupling F-actin polymerization to the membrane of the bacteriogenic protocells or embedded vacuoles using proteins such as Sla2 or HIP1R[34] could lead to life-like microdevices with mechanically responsive properties. Moreover, a first step to a synthetic cell with rudimentary 'proto-eukaryote' characteristics would be realized if the DNA–histone proto-nuclei could be used as a dynamic repository for controlling downstream information processing.

As coacervate-based microencapsulation is known to increase the viability of probiotics[35], it should be possible to use engineered

bacteria to deliver specialized components and biological processes for establishing robust metabolic networks and genetic circuitry in the bacteriogenic protocells. Thus, we expect that the methodology will be responsive to high levels of programmability. For example, combinations of engineered strains such as *Komagataeibacter rhaeticus* and *Zymomonas mobilis*, which are capable of high cellulose production[36] and cellulolytic activity[37], respectively, could be used to deliver and implement on-site synergistic metabolic networks of ethanol production for biofuels and food processing. Moreover, new types of self-powered metabolic networks could be assembled inside the bacteriogenic protocells by in situ lysis of bacteria such as *Photobacterium phosphoreum* to charge the cytoplasmic-like medium with appropriate molecular machinery for bioluminescence. Such advances will require increased levels of stability and homogeneity in the populations of bacteriogenic protocells currently produced, as well as overcoming current limitations placed on the reproducible scale-up of the living-material assembly process.

Finally, from a cellular bionic perspective, the potential for symbiosis in living/synthetic cell hybrids constructed from bacterially derived construction pathways could offer more complex modules for development in diagnostic and therapeutic areas of synthetic biology as well as in biomanufacturing and biotechnology in general. For example, implantation of live photosynthetic bacteria or sulfate-reducing bacteria within the bacteriogenic protocells in place of *E. coli* cells could offer new strategies for operating the cellular bionic systems under photochemical or anaerobic conditions, respectively. Alternatively, bacterially derived bioluminescence could provide light energy for powering live photosynthetic purple bacteria implanted in the bacteriogenic protocells, and the corresponding production of oxygen and carbohydrates from the surrogate chloroplasts could be used for extracellular ATP production in co-implanted live *E. coli* cells, which in turn act as surrogate mitochondria. Coupling these endogenous circuits to diagnostic functions towards cytokines, hormones and metabolites will be challenging, ultimately relying on the high capture efficiency of the internal coacervate matrix and appropriate design of the output signals through judicious engineering of the living/synthetic cell interface.

Online content

Any methods, additional references, Nature Research reporting summaries, source data, extended data, supplementary information, acknowledgements, peer review information; details of author contributions and competing interests; and statements of data and code availability are available at https://doi.org/10.1038/s41586-022-05223-w.

1. van Stevendaal, M. H. M. E., van Hest, J. C. M. & Mason, A. F. Functional interactions between bottom-up synthetic cells and living matter for biomedical applications. *ChemSystemsChem* **3**, e2100009 (2021).
2. Jeong, S., Nguyen, H. T., Kim, C. H., Ly, M. N. & Shin, K. Toward artificial cells: novel advances in energy conversion and cellular motility. *Adv. Funct. Mater.* **30**, 1907182 (2020).
3. Toparlak, O. D. & Mansy, S. S. Progress in synthesizing protocells. *Exp. Biol. Med.* **244**, 304–313 (2018).
4. Yewdall, N. A., Mason, A. F. & van Hest, J. C. M. The hallmarks of living systems: towards creating artificial cells. *Interface Focus* **8**, 20180023 (2018).
5. Adamala, K. P., Martin-Alarcon, D. A., Guthrie-Honea, K. R. & Boyden, E. S. Engineering genetic circuit interactions within and between synthetic minimal cells. *Nat. Chem.* **9**, 431–439 (2017).
6. Deng, N.-N., Yelleswarapu, M., Zheng, L. & Huck, W. T. S. Microfluidic assembly of monodisperse vesosomes as artificial cell models. *JACS* **139**, 587–590 (2017).
7. Weiss, M. et al. Sequential bottom-up assembly of mechanically stabilized synthetic cells by microfluidics. *Nat. Mater.* **17**, 89–96 (2018).
8. Huang, X. et al. Interfacial assembly of protein–polymer nano-conjugates into stimulus-responsive biomimetic protocells. *Nat. Commun.* **4**, 2239 (2013).
9. Li, M., Harbron, R. L., Weaver, J. V. M., Binks, B. P. & Mann, S. Electrostatically gated membrane permeability in inorganic protocells. *Nat. Chem.* **5**, 529–536 (2013).
10. Marguet, M., Bonduelle, C. & Lecommandoux, S. Multicompartmentalized polymeric systems: towards biomimetic cellular structure and function. *Chem. Soc. Rev.* **42**, 512–529 (2013).
11. Niederholtmeyer, H., Chaggan, C. & Devaraj, N. K. Communication and quorum sensing in non-living mimics of eukaryotic cells. *Nat. Commun.* **9**, 5027 (2018).
12. Kumar, B. V. V. S. P., Patil, A. J. & Mann, S. Enzyme-powered motility in buoyant organoclay/DNA protocells. *Nat. Chem.* **10**, 1154–1163 (2018).
13. Mukwaya, V. et al. Lectin-glycan-mediated nanoparticle docking as a step toward programmable membrane catalysis and adhesion in synthetic protocells. *ACS Nano* **14**, 7899–7910 (2020).
14. Dou, H. et al. Higher-order assembly of crystalline cylindrical micelles into membrane-extendable colloidosomes. *Nat. Commun.* **8**, 426 (2017).
15. Martin, N. Dynamic synthetic cells based on liquid–liquid phase separation. *ChemBioChem* **20**, 2553–2568 (2019).
16. Zhang, Y. et al. Giant coacervate vesicles as an integrated approach to cytomimetic modeling. *JACS* **143**, 2866–2874 (2021).
17. Tang, T.-Y. D. et al. Fatty acid membrane assembly on coacervate microdroplets as a step towards a hybrid protocell model. *Nat. Chem.* **6**, 527–533 (2014).
18. Koga, S., Williams, D. S., Perriman, A. W. & Mann, S. Peptide–nucleotide microdroplets as a step towards a membrane-free protocell model. *Nat. Chem.* **3**, 720–724 (2011).
19. Tang, T.-Y. D., van Swaay, D., deMello, A., Ross Anderson, J. L. & Mann, S. In vitro gene expression within membrane-free coacervate protocells. *Chem. Commun.* **51**, 11429–11432 (2015).
20. Li, M., Green, D. C., Anderson, J. L. R., Binks, B. P. & Mann, S. In vitro gene expression and enzyme catalysis in bio-inorganic protocells. *Chem. Sci.* **2**, 1739–1745 (2011).
21. Küchler, A., Yoshimoto, M., Luginbühl, S., Mavelli, F. & Walde, P. Enzymatic reactions in confined environments. *Nat. Nanotechnol.* **11**, 409–420 (2016).
22. Strulson, C. A., Molden, R. C., Keating, C. D. & Bevilacqua, P. C. RNA catalysis through compartmentalization. *Nat. Chem.* **4**, 941–946 (2012).
23. Drobot, B. et al. Compartmentalised RNA catalysis in membrane-free coacervate protocells. *Nat. Commun.* **9**, 3643 (2018).
24. Faust, J. E., Yang, P.-Y. & Huang, H. W. Action of antimicrobial peptides on bacterial and lipid membranes: a direct comparison. *Biophys. J.* **112**, 1663–1672 (2017).
25. Gray, L. R., Tompkins, S. C. & Taylor, E. B. Regulation of pyruvate metabolism and human disease. *Cell. Mol. Life Sci.* **71**, 2577–2604 (2014).
26. Silverman, A. D., Karim, A. S. & Jewett, M. C. Cell-free gene expression: an expanded repertoire of applications. *Nat. Rev. Genet.* **21**, 151–170 (2020).
27. Lee, K. Y. et al. Photosynthetic artificial organelles sustain and control ATP-dependent reactions in a protocellular system. *Nat. Biotechnol.* **36**, 530–535 (2018).
28. Fung, B. M. & Eyob, E. The effect of ATP concentration on the rate of actin polymerization. *Arch. Biochem. Biophys.* **220**, 370–378 (1983).
29. Nakashima, K. K., Baaij, J. F. & Spruijt, E. Reversible generation of coacervate droplets in an enzymatic network. *Soft Matter* **14**, 361–367 (2018).
30. Mempin, R. et al. Release of extracellular ATP by bacteria during growth. *BMC Microbiol.* **13**, 301 (2013).
31. Alvarez, C. L. et al. Dynamic regulation of extracellular ATP in *Escherichia coli*. *Biochem. J.* **474**, 1395–1416 (2017).
32. Donau, C. et al. Active coacervate droplets as a model for membraneless organelles and protocells. *Nat. Commun.* **11**, 5167 (2020).
33. Moreau, N. G., Martin, N., Gobbo, P., Tang, T. Y. D. & Mann, S. Spontaneous membrane-less multi-compartmentalization via aqueous two-phase separation in complex coacervate micro-droplets. *Chem. Commun.* **56**, 12717–12720 (2020).
34. Skruzny, M. et al. Molecular basis for coupling the plasma membrane to the actin cytoskeleton during clathrin-mediated endocytosis. *Proc. Natl Acad. Sci. USA* **109**, E2533–E2542 (2012).
35. Bosnea, L. A., Moschakis, T. & Biliaderis, C. G. Complex coacervation as a novel microencapsulation technique to improve viability of probiotics under different stresses. *Food Bioprocess Technol.* **7**, 2767–2781 (2014).
36. Florea, M. et al. Engineering control of bacterial cellulose production using a genetic toolkit and a new cellulose-producing strain. *Proc. Natl Acad. Sci. USA* **113**, E3431–E3440 (2016).
37. Linger, J. G., Adney, W. S. & Darzins, A. Heterologous expression and extracellular secretion of cellulolytic enzymes by *Zymomonas mobilis*. *Appl. Environ. Microbiol.* **76**, 6360–6369 (2010).

Methods

Materials

The following chemicals were used as received: PDDA (Sigma-Aldrich, 20 wt% in H_2O, molecular mass = 8.5, 100–200 or 400–500 kDa), ATP, UTP, fluorescein isothiocyanate (FITC), rhodamine B isothiocyanate (RITC; mixed isomers), FITC–CM-dextran (molecular mass = 4, 70 or 150 kDa), FITC-dextran (molecular mass of 4 kDa), poly(allylamine hydrochloride) (PAH, molecular mass = 50 kDa), bovine serum albumin (BSA), sulforhodamine B (Sul-RhB), calcein, Nile Red, DAPI, 8-hydroxypyrene-1,3,6-trisulfonic acid trisodium salt, RBG, lysozyme from chicken egg white (≥90%), melittin from honey bee venom (≥85%, HPLC), deoxyribonucleic acid (low molecular mass from salmon sperm), deoxyribonucleic acid (DNA) sodium salt from *Escherichia coli* strain B (genomic, unsheared), histone from calf thymus (type II-A, molecular mass of 14.0 kDa, lyophilized powder), ethylenediaminetetraacetic acid (EDTA), PK, PEP, adenosine diphosphate (ADP), dimethyl sulfoxide (DMSO), glutaraldehyde, sodium cacodylate trihydrate, Tris(hydroxymethyl)aminomethane, Tris-base, glycine, sodium dodecyl sulfate (SDS), carbenicillin, Millipore PVDF Membranes, Tween-20, SiO_2 microspheres (2 μm), polystyrene beads (1 μm), polystyrene beads (3 μm), polystyrene beads (5 μm), amine-modified polystyrene beads (2 μm), carboxylate-modified polystyrene beads (2 μm), (3-aminopropyl)triethoxysilane, trimethoxy(octadecyl)silane, tri(*N*-acetyl-D-glucosamine) (NAG3), 3-(4-octadecyl)benzoylacrylic acid (OBAA), resorufin, fluorescein, luciferase from *Photinus pyralis* (firefly), D-luciferin, propylene glycol methyl ether acetate, BCA Protein Assay Kit, 1,4-dithiothreitol, 2-mercaptoethanol, peptone from casein and other animal proteins, glucose, peptone and yeast extract were purchased from Sigma-Aldrich. SYTO-9, propidium iodide (PI), DiI stain (1,1′-dioctadecyl-3,3,3′,3′-tetramethylindocarbocyanine perchlorate (DiIC18(3)), DNase I (DNase I buffer and $MnCl_2$ solution were included), Molecular Probes EnzChek Lipase Substrate (green fluorescent, 505/515 substrate, lipase), Molecular Probes EnzChek Protease Assay Kit (green fluorescence, 100 to 1000 assays kit), BODIPY FL NHS Ester, MTT (3-(4,5-dimethylthiazol-2-yl)-2,5-diphenyltetrazolium Bromide), NuPage Sep Tris-glycine gels (4–15 wt%), Expressway Mini Cell-Free Expression System kit, Qubit dsDNA BR Assay Kit, Qubit RNA HS Assay Kit, Z′-LYTE Kinase Assay Kit (Ser/Thr 5 Peptide) and DyLight 550 NHS Ester were purchased from Thermo Fisher Scientific. 2-[Methoxy(polyethyleneoxy) propyl] trimethoxysilane (PEGsilane) was purchased from ABCR, 90%). Fluorescein diphosphate was purchased from Insight Biotechnology. The QIAprep Spin Miniprep Kit (MINIPREP) was purchased from Qiagen. The EnzyChrom Glycolysis Assay Kit was purchased from BioAssay Systems; actin protein (rhodamine, actin-RhB, rabbit skeletal muscle, >99%) was purchased from Universal Biologicals. The free fatty acid assay kit, anti-GFP antibodies (chicken) and goat anti-chicken IgY H&L (alkaline phosphatase) were purchased from Abcam. CM-dextran (molecular mass of 70 kDa) was purchased from Carbosynth. Single-stranded DNA oligonucleotides (23 nucleotides in length, GTTAGCAGCCGGATCTCAGTGGT) with 3′-TAMRA or 3′-FAM (ssDNA-FAM) modifications were purchased from Integrated DNA Technologies. The oligonucleotides were HPLC purified and freeze-dried by the supplier. Oligonucleotides were used as provided and dissolved in nuclease-free buffer (50 mM Tris-HCl, 100 mM NaCl, pH 7.4) to give stock solutions of 100 μM. Skimmed milk was purchased from the local supermarket. Ethanol, methanol and toluene were obtained from the chemical store at the School of Chemistry, University of Bristol. LB agar plates and broth, 2× YT agar plates and broth, 2% agarose gel and phosphate-buffered saline (PBS) were obtained from general laboratory supplies of the School of Cellular and Molecular Medicine, University of Bristol. All of the bacteria strains—*Escherichia coli* (*E. coli*; strain BL21(DE3) or strain Rosetta(DE3)), *P. aeruginosa* (strain PAO1) and *Staphylococcus aureus*—were provided by the group of J. Spencer and used as received. Purified eGFP protein and purified mCherry protein was provided by A. Coutable from the group of J. L. R. Anderson. deGFP protein was purified and provided as a gift by J. Spencer.

Preparation of coacervate microdroplets

Typically, positively charged microdroplet dispersions were prepared at a PDDA/ATP monomer molar ratio of 2:1 by adding an aqueous solution of ATP (20 mM, pH 8.0) to the same volume of an aqueous solution of PDDA (monomer concentration, 40 mM; pH 8.0) with molecular masses of 8.5, 100–200 or 400–500 kDa. The dispersions were centrifuged (Eppendorf microcentrifuge, 5415D) under 15,000 rcf for 5 min, and were then redispersed with a pipette before use. Similar procedures were used to prepare PDDA/UTP coacervate microdroplets by adding an aqueous solution of UTP (20 mM, pH 8.0) to the same volume of an aqueous solution of PDDA (molecular mass of 8.5 kDa, monomer concentration, 40 mM; pH 8.0).

Bacterial cultures

The following bacterial cultures were used: *E. coli* (strain BL21(DE3) or strain Rosetta(DE3)) and *P. aeruginosa* (strain PAO1). Typically, glycerol stocks (kept at −70 °C) of bacteria were freshly streaked on agar plates (1.6% agar) once a month. Single colonies taken from the agar plate were grown overnight in culture broth under 37 °C and 500 rpm. For *E. coli* BL21(DE3) and *P. aeruginosa*, LB agar plates and broth were used, whereas 2× YT agar plates and broth were used for *E. coli* Rosetta(DE3). The overnight cultures were regrown by diluting 100:1 in fresh LB broth (grown to an optical density at 600 nm (OD_{600}) of 0.3–0.5), then chilled in ice for 30 min and centrifuged (at 4 °C and 4,000 rpm) for 5 min, followed by transfer to the medium used for the experiments.

Coacervate droplet-mediated compartmentalization of bacterial colonies

An aqueous coacervate dispersion (typically PDDA/ATP or PDDA/UTP, concentrations as described above) was centrifuged and half of the volume of the supernatant was removed (typically 50 μl) and added to a sample tube containing a solution (10 μl) of a single strain of bacteria (*E. coli* or *P. aeruginosa*; OD_{600} = 20) or a suspension of both *E. coli* and *P. aeruginosa* (OD_{600} = 20; $OD_{E.\ coli}$:$OD_{P.\ aeruginosa}$ = 2:1). The mixture was then added to the coacervate dispersion, mixed gently with a pipette to redisperse the coacervate phase into microdroplets, and the bacteria-containing suspension was incubated for 3 min at room temperature. Alternatively, 40 μl of a redispersed coacervate solution was removed and added to the cavity of a PEGsilane-functionalized O-slide. After allowing the drops to settle for 3 min, 5 μl of bacteria (OD_{600} = 20) was added to coacervate droplet suspension.

Zeta potential and contact-angle measurements

All zeta potential measurements were performed using a Malvern Zetasizer Nano-ZS instrument equipped with an internal Peltier temperature controller. Samples were injected into a disposable zeta cuvette and experiments were carried out at 25 °C. Contact-angle measurements were performed using KRÜSS Drop Shape Analyzer DSA100 instrument. All of the samples were dried and coated on a flat glass surface. Typically, the water drop volume was 2.0 μl.

FACS analysis

For analysis of bacterial cell partitioning in coacervate droplets, FACS experiments were performed on a BD LSRFortessa X-20 cell analyzer with BD FACS Diva software. A coacervate or coacervate/ssDNA–TAMRA droplet suspension (200 μl) was added to the FACS tube, and 2 μl of a single strain of bacteria or a mixture of bacterial strains (initial OD_{600} = 20, final OD_{600} = 0.2) or a bacterial lysate was added. For samples with dyes, the final dye concentrations were as follows: ssDNA–TAMRA (2.5 μM), SYTO-9 (0.2 μM), DiI (0.2 μg ml^{-1}). Coacervate/ssDNA–TAMRA droplets were prepared by adding 0.5 μl of ssDNA-TAMRA (1 mM) to

200 µl of a coacervate dispersion, followed by centrifugation and redispersion before use. The following lasers and filters were used: SYTO-9 and eGFP: laser 488 nm, filter 530/30 nm; TAMRA and DiI: laser 561 nm, filter 586/15 nm; mCherry: laser 561 nm, filter 610/20 nm. For bacterial viability (live/dead) monitoring and proliferation counting in protocells, FACS experiments were performed on the Acea NovoCyte flow cytometer with the NovoExpress software. Typically, 200 µl of samples with protocells stained by SYTO-9 (1 µM) and PI (5 µM) were added to a sample tube. The following lasers and filters were used: SYTO-9: laser 488 nm, filter 530/30 nm; PI: laser 561 nm, filter 780/60 nm.

Construction of bacteriogenic coacervate-based protocells

Reconfiguration of PDDA/ATP or PDDA/UTP coacervate droplets loaded and coated with *E. coli* or *P. aeruginosa* cells, respectively, into cell-membrane-enclosed metabolically active synthetic cells was achieved by in situ lysis of the captured bacteria. For this, a solution of lysozyme (5 mg ml^{-1} in 20 mM Tris-HCl, 2 mM EDTA, pH 8.0 buffer) and melittin (2 mg ml^{-1}) was added to 0.05 ml of a suspension of the bacteria-containing coacervate microdroplets. In some of the experiments, *E. coli* cultures were pretreated with lysozyme (20 mg ml^{-1} in buffer) for 3.5 h before capture along with *P. aeruginosa* by the coacervate droplets to increase their sensitivity to the subsequent lysozyme/melittin treatment such that both *E. coli* and *P. aeruginosa* cells released their contents at similar in situ rates during the construction of the synthetic protocells (*E. coli* cells pretreated in this way with lysozyme did not undergo lysis but were compromised in their cell wall integrity such that they became more sensitive to melittin-induced disassembly). In general, the protocells were left in the lysis solution and fresh samples were used for the experiments. Alternatively, excess bacterial lysate and non-lysed bacteria were removed by carefully exchanging the top layer of the suspension with a supernatant obtained from a corresponding coacervate suspension obtained after centrifugation. The samples were not extensively washed owing to their mechanical fragility and sensitivity to changes in osmotic pressure.

Determination of bacterial lysis and death ratios

Bacterial cell lysis ratios (L) were determined from measurements of OD_{600} recorded before and after treatment with lysozyme and/or melittin ($L = OD_{600}$ (after)/OD_{600} (before)). Bacterial cell death ratios (D) were determined by using a tetrazolium salt (MTT) colorimetric assay in which *E. coli* BL21 (DE3) cells before and after treatment with 2 mg ml^{-1} of melittin were incubated with MTT in a microdilution plate at 36–37 °C for different time periods. DMSO was added as a formazan dissolvent, and the mixtures were measured for OD_{510} or absorbance at 510 nm (A_{510}; $D = A_{510}$ (after)/A_{510} (before).

Fluorometric quantification of released proteins and DNA

To determine the concentrations of eGFP, mCherry and DNA released by bacteria after lysis into the coacervate phase, samples were centrifuged under 15,000 rcf for 5 min and the aqueous supernatant was removed. The remaining coacervate phase was then disassembled by dilution 1,000 times using PBS and the corresponding fluorescence intensities were determined using a plate reader. Protein concentrations were obtained from calibration curves using known standards. DNA concentrations were determined using the Qubit dsDNA BR Assay Kit[38]. Standard samples with known concentrations were prepared using purified eGFP protein (0–1 µg ml^{-1}; excitation at 400 nm, emission at 510 nm), purified mCherry protein (0–1 µg ml^{-1}; excitation at 587 nm, emission at 610 nm) and commercial *E. coli* DNA (0–1 µg ml^{-1}; excitation at 535 nm, emission at 617 nm). All of the proteins and DNA were dissolved in PBS and fluorescence intensities were recorded using the plate reader.

SEM analysis

For imaging coacervate droplets with microcompartmentalized bacterial colonies, samples of *E. coli* and *P. aeruginosa* were fixed with glutaraldehyde before capture. Bacterial cells were washed twice in 0.1 M sodium cacodylate buffer, and then fixed with 2.5% glutaraldehyde in sodium cacodylate buffer (0.1 M) for 2 h. After rinsing with water, 5 µl of the bacteria-containing mixture (OD_{600} = 20) were added to 40 µl of a PDDA/ATP coacervate and dropped onto the cut pegylation coverslips that were attached to a scanning electron microscopy (SEM) sample stage. The sample was incubated for 10 min and then freeze-dried for SEM analysis. The bacterial lysate containing coacervate droplets was also prepared without fixation. In this case, droplets of the sample were mounted onto cut pegylation coverslips attached to the SEM sample stage and then freeze-dried. All of the SEM experiments were performed on the Jeol IT300 SEM instrument.

Quantification of biological components in bacteriogenic protocells

Bacteriogenic coacervate-based protocells were disassembled by dilution 1,000 times using PBS. DNA, RNA, protein and lipid concentrations were determined using the Qubit dsDNA BR assay kit[38], Qubit RNA HS assay kit[39], BCA protein assay kit[40] and free fatty acid assay kit[41], respectively. The mass of water (M_{water}) contained in the protocells was determined by the difference between the wet mass (M_{wet}) and the dry mass of the protocell (M_{dry}). The mass of residual components was determined by $M_{dry} - (M_{DNA} + M_{RNA} + M_{protein} + M_{lipids})$.

Proteomics of bacteriogenic protocells

Bacteriogenic coacervate-based protocells were prepared with *E. coli* BL21(DE3) and PAO1 cellular constituents and washed three times with supernatant obtained from a PDDA/ATP coacervate suspension to remove non-associated bacterial proteins. For comparison, a dataset was obtained from a binary population of *E. coli* (strain BL21 (DE3; OD_{600} = 2) and *P. aeruginosa* (strain PAO1, OD = 1) cells prepared without the coacervate droplets. The mixture was incubated overnight with lysozyme (20 mg ml^{-1} in 20 mM Tris-HCl, 2 mM EDTA, pH 8.0 buffer) and then centrifuged under 2,000 rpm for 10 min followed by washing with PBS to remove residual lysozyme. The bacterial cells were then lysed by using a freeze–thaw method involving ten cycles, and then analysed using LC–MS.

For nano-LC–MS, the samples were run on a 10% SDS–PAGE gel until the dye front had migrated approximately 1 cm into the separating gel. Each gel lane was then excised as a single slice and processed for in-gel tryptic digestion using the DigestPro automated digestion unit (Intavis).

The resulting peptides were fractionated using the Ultimate 3000 nano-LC system in line with an Orbitrap Fusion Tribrid mass spectrometer (Thermo Fisher Scientific). Peptides in 1% (v/v) formic acid were injected onto the Acclaim PepMap C18 nano-trap column (Thermo Fisher Scientific). After washing with 0.5% (v/v) acetonitrile 0.1% (v/v) formic acid, the peptides were resolved on a 250 mm × 75 µm Acclaim PepMap C18 reverse-phase analytical column (Thermo Fisher Scientific) over a 150 min organic gradient, using seven gradient segments (1–6% solvent B over 1 min, 6–15% B over 58 min, 15–32% B over 58 min, 32–40% B over 5 min, 40–90% B over 1 min, held at 90% B for 6 min and then reduced to 1% B over 1 min) with a flow rate of 300 nl min^{-1}. Solvent A was 0.1% formic acid and solvent B was aqueous 80% acetonitrile in 0.1% formic acid. Peptides were ionized by nano-electrospray ionization at 2.2 kV using a stainless-steel emitter with an internal diameter of 30 µm (Thermo Fisher Scientific) and a capillary temperature of 250 °C.

All spectra were acquired using an Orbitrap Fusion Tribrid mass spectrometer controlled by Xcalibur v.2.1 software (Thermo Fisher Scientific) and operated in data-dependent acquisition mode. FTMS1 spectra were collected at a resolution of 120,000 over a scan range (m/z) of 350–1,550, with an automatic gain control (AGC) target of 400,000 and a max injection time of 100 ms. Precursors were filtered according to charge state (to include charge states 2–7), with monoisotopic peak determination set to peptide and using an intensity range from 5×10^3

to 1×10^{20}. Previously investigated precursors were excluded using a dynamic window (40 s, ±10 ppm). The MS2 precursors were isolated with a quadrupole mass filter set to a width of 1.6 *m*/*z*. ITMS2 spectra were collected with an AGC target of 5,000, a max injection time of 50 ms and HCD collision energy of 35%.

The raw data files were processed and quantified using Proteome Discoverer software v.2.1 (Thermo Fisher Scientific) and searched against the UniProt *E. coli* (strain BL21-DE3) database (downloaded November 2020; 4,156 sequences) and the UniProt *P. aeruginosa* PAO1 database (downloaded November 2020; 5,563 sequences) using the SEQUEST HT algorithm. Peptide precursor mass tolerance was set at 10 ppm, and MS/MS tolerance was set at 0.6 Da. Search criteria included oxidation of methionine (+15.995 Da), acetylation of the protein N terminus (+42.011 Da) and methionine loss plus acetylation of the protein N terminus (−89.03 Da) as variable modifications, and carbamidomethylation of cysteine (+57.021 Da) as a fixed modification. Searches were performed with full tryptic digestion and a maximum of two missed cleavages were allowed. The reverse database search option was enabled and all data were filtered to satisfy a false-discovery rate of 5% (see Source Data file for Fig. 2).

Enzyme and glycolysis activities in bacteriogenic protocells

Activities of alkaline phosphatase, protease and lipase within the bacteriogenic protocells were determined by fluorescence microscopy at room temperature using fluorescein diphosphate (green fluorescence), EnzChek Protease Substrate (green fluorescence) or EnzChek Lipase Substrate (green fluorescence). An aqueous solution of a single substrate (final concentration, 0.2 mg ml^{-1}) was added to a suspension of the protocells and the enzyme-mediated production of the fluorescence output was monitored by using confocal microscopy.

The activity of β-gal in the protocells was determined using the resorufin β-D-galactopyranoside (RBG) reaction test. Time-dependent fluorescence profiles were recorded by fluorescence spectroscopy from a suspension of coacervate droplets (40 µl) containing PAO1 and *E. coli* Rosetta(DE3) cells before and after lysis in the presence of RBG (5 µl, 2 mM) (excitation: 560 nm, emission: 594 nm). The reactions were also monitored using wide-field (excitation: 545/26 nm emission: 605/70 nm) and confocal (excitation: 560 nm, emission: 571–621 nm) microscopes.

Glycolysis assays were performed using the EnzyChrom Glycolysis Assay Kit with a conversion of 1 mM L-lactate equal to 9.01 mg dl^{-1} (90.1 ppm)[42].

Construction of plasmid pEXP5-NT/deGFP

The *deGFP* gene was amplified from *E. coli* Rosetta(DE3) cells and inserted into the plasmid pEXP5-NT/CALML3 (obtained from the Expressway Mini Cell-Free Expression System kit, Thermo Fisher Scientific) using ligase-independent cloning to yield the plasmid pEXP5-NT/deGFP[43]. Primers were designed to facilitate the replacement of the *CALML3* gene with the *deGFP* gene. The plasmid retained the ampicillin-resistance gene, T7 promoter site, ribosome-binding site and the pUC origin of replication sequence. The constructed plasmid pEXP-NT/deGFP was then transformed into *E. coli* BL21 competent cells for amplification. The BL21 cells were isolated by centrifugation and smeared onto an agar plate containing the antibiotic carbenicillin and incubated overnight at 37 °C. A single colony was removed from the agar and incubated in LB broth with carbenicillin overnight at 37 °C. The cells were collected and the plasmid was extracted from the *E. coli* cells and purified using the Miniprep kit (Qiagen) resulting in a final plasmid concentration of 219 ng $µl^{-1}$.

Endogenous gene expression in bacteriogenic protocells

The plasmid pEXP5-NT/deGFP (final concentration, 1 µg per 100 µl), as well as buffer, promoters for T7 polymerases (sequence: TAATACGACTCACTATAGGG) and nutrients from the Expressway Mini Cell-Free Expression System kit (Thermo Fisher Scientific) were added to a PDDA/ATP coacervate suspension before capture of the bacteria. The added components included 2.5× IVPS *E. coli* reaction buffer (5 µl; no amino acids), T7 enzyme mix (1 µl), an amino acid mix (1 µl, 50 mM, no methionine) and methionine (1 µl, 75 mM), all per 100 µl of the protocell suspension. No bacterial lysate from the cell-free expression kit was added such that all the gene expression machinery in the protocells was derived from the in situ lysis of the captured bacterial cells. Bacteriogenic protocells were then prepared using the above coacervate/component droplet suspension by in situ lysis of the captured *P. aeruginosa* (strain PAO1) and *E. coli* (strain Rosetta(DE3)) cells. The samples were mounted on an O-slide for microscopy experiments or used directly for protein electrophoresis and western blot analysis. All of the experiments were undertaken at 37 °C for periods of 3 h (microscopy) or 12 h (protein electrophoresis/western blot). The samples were initially kept on ice and then raised to a temperature of 37 °C to initiate in vitro gene expression. After the first 30 min, a supplement of 2 µl per 100 µl of the 2× IVPS feed buffer was added.

Protein gel electrophoresis and western blot analysis

For protein electrophoresis, protocell samples were disassembled by addition of 100 mM NaCl to release all of the proteins from the coacervate phase. Then, 10 µl of the sample solution and sample application buffer were loaded into NuPage Sep Tris-glycine gels 4–15 wt% (Thermo Fisher Scientific) and separated based on protein molecular mass using a constant voltage of 200 mV for 35 min. The gels were washed by water, stained overnight in staining solution under shaking, and then destained by water for 24 h to remove excess dye from the gel matrix background. Western blot analysis was performed as follows. After protein electrophoresis, the protein was transferred from the gel using a transfer buffer (containing 390 mM glycine, 478 mM Tris-Base, 13 mM SDS, 20% methanol) onto a methanol-activated PVDF membrane (Millipore) at a constant current of 45 mA for 1 h. The PVDF membrane was blocked using casein (skimmed milk) for 1.5 h at room temperature and then incubated with monoclonal anti-GFP (rabbit) antibodies (1 µg ml^{-1}) (Sigma-Aldrich) for 1 h at room temperature. The PVDF membrane was then washed at least five times with PBS-Tween-20 (0.1%) with 20 min shaking between each rinse before film exposure and development.

Fluorometric quantification of enzyme products and expressed protein deGFP

To determine the concentrations of fluorescence enzyme products and expressed protein deGFP, the bacteriogenic protocells were centrifugated at 15,000 rcf for 5 min. The sedimented protocells and aqueous supernatant were collected. The volume of protocells ($V_{protocell}$) was calculated by $V_{total} - V_{supernatant}$, where V_{total} is the total volume of the sample, and $V_{supernatant}$ is the volume of supernatant. The protocells were then disassembled by dilution 1,000 times using PBS.

The fluorescence intensities associated with the protocells or supernatant were measured using a plate reader. The enzyme products and protein deGFP concentrations were calculated from calibration curves using known standards. Standards with known concentrations were prepared by using resorufin (β-gal product, excitation: 560 nm, emission: 594 nm, 0–10 µM), fluorescein (alkaline phosphatase product, excitation: 488 nm, emission: 520 nm, 0–10 µM), free BODIPY FL dye (lipase and protease products, excitation: 494 nm, emission: 520 nm, 0–10 µM) and purified deGFP protein (excitation at 485 nm, emission at 528 nm, 0–0.1 µM).

The total amount of enzyme products and expressed protein deGFP in the protocells or supernatants was calculated by $C \times V$, where C is the concentration of enzyme products or deGFP, and V is the volume of the protocells or supernatant.

In situ proto-nucleus formation in bacteriogenic coacervate-based protocells

Aqueous solutions of PDDA (40 mM, 50 µl), ATP (20 mM, 50 µl), melittin (20 mg ml^{-1}, 10 µl), histone (20 mg ml^{-1}, 10 µl), DNase I (1 U $µl^{-1}$, 5 µl)

and $MnCl_2$ (100 mM, 1 µl) were mixed to produce a four-component coacervate. After centrifugation under 15,000 rcf for 5 min, 40 µl of the redispersed coacervate suspension was removed and added to the cavity of a PEGsilane-functionalized O-slide. *E. coli* cells (OD_{600} = 20) were pretreated with lysozyme (20 mg ml^{-1} in 20 mM Tris-HCl, 2 mM EDTA, pH 8.0 buffer) for 3.5 h and mixed with a *P. aeruginosa* colony (OD_{600} = 20) at a volume ratio of 2: 1. The bacteria mixture (5 µl) was then added to the PDDA/ATP/melittin/histone/DNase I coacervate phase in the O-slide, and lysozyme and melittin were added to give final concentrations of 2 mg ml^{-1}. The resulting mixture was sealed with a cover slide and incubated at 37 °C for 1 h to induce cell lysis, capture of the bacterial components in the coacervate droplets and DNase-mediated fragmentation of the release plasmids into linear substrands, followed by addition of 5 µl of 1,4-dithiothreitol (1 mM) and 2-mercaptoethanol (0.5 mM) and incubation for another 1 h to inactivate the DNase I. After incubation, FITC–CM-dextran (10 µl, 10 mg ml^{-1}) was gently added to the mixture to induce phase separation of the DNA fragments in the form of a single DNA–histone subcompartment within the coacervate phase.

DyLight 550 labelling of bacterial proteins

A bacterial lysate was prepared by adding lysozyme (20 mg ml^{-1} in 20 mM Tris-HCl, 2 mM EDTA, pH 8.0 buffer) to a mixture of *E. coli* strain BL21(DE3) (OD = 2) and *P. aeruginosa strain PAO1* (OD = 1), and incubating overnight. The bacteria were then centrifugated under 2,000 rpm for 10 min and washed with PBS to remove the lysozyme, and the cells were lysed using a freeze–thaw method involving ten cycles of freezing by liquid nitrogen and thawing in a water bath set at 37 °C. Then, 40 µl of DyLight 550 NHS Ester (dissolved in DMSO, 1 mg ml^{-1}) was added dropwise to 2 ml of the bacterial lysate (in 100 mM $NaHCO_3/Na_2CO_3$ buffer, pH 9.0), followed by stirring for 12 h in the dark at 4 °C. The mixed solution was then placed in a filter bag and dialysed against PBS (0.01 M PBS, pH 7.4) and then against H_2O at 4 °C in the dark for 2 days. The resulting solution was centrifugated at 13,000 rpm for 10 min to remove any insoluble precipitate and then freeze-dried.

Partitioning of bacterial proteins in protocells

DyLight-550-labelled bacterial proteins (20 mg ml^{-1}, 10 µl) were added to a suspension (40 µl) of bacteriogenic protocells containing a DNA–histone subcompartment, and partitioning between the proto-cytoplasmic and proto-nucleus regions was recorded by confocal microscopy.

Synthesis of FITC/RITC-labelled proteins and polymers

FITC or RITC (200 µl; dissolved in DMSO, 1 mg ml^{-1}) was added drop by drop to 10 ml of a protein or polymer (10 mg ml^{-1}, dissolved in 100 mM $NaHCO_3/Na_2CO_3$ buffer, pH 9.0) solution, followed by stirring for 12 h in the dark at 4 °C. The mixed solution was next placed in dialysis tubing and dialysed against PBS (0.01 M PBS, pH 7.4) and then H_2O at 4 °C in the dark for 2 days. The resulting solution was centrifuged at 13,000 rpm for 10 min to remove any insoluble precipitate and then freeze-dried.

In situ assembly of F-actin in bacteriogenic protocells

Remodelled PDDA/ATP coacervate-based bacteriogenic protocells comprising a DNA–histone-enriched phase-separated subcompartment were prepared as described above and an aqueous solution of rhodamine-B-labelled G-actin (final concentration, 50 µg ml^{-1}) was added to the protocell suspension followed by a F-actin-initiator buffer (500 mM KCl, 20 mM $MgCl_2$ in 100 mM Tris, pH 7.5) such that the system was activated by the coacervate ATP. A non-active system was established by preparing the bacteriogenic protocells as described above but using UTP instead of ATP as the main component of the coacervate followed by addition of G-actin and the Mg^{2+}-containing buffer. Alternatively, an ATP-generation system (PK (0.2 mg ml^{-1}), PEP (10 mM) and ADP (10 mM)) was preloaded into the coacervate droplets before protocell construction and G-actin/Mg^{2+} was then added to control intraprotocell cytoskeletal assembly.

Live-cell energization of bacteriogenic protocells

Bacteriogenic protocells based on PDDA/UTP coacervate droplets and containing a DNA–histone proto-nucleus were constructed as described above but using only half of the *P. aeruginosa* colony to give a volume ratio of *E. coli* (OD_{600} = 20):*P. aeruginosa* (OD_{600} = 10) of 2:1. The resulting protocells were enclosed by an incomplete outer membrane, enabling subsequent uptake of live *E. coli* cells. An aqueous mixture of a lysozyme inhibitor (NAG3, 10 mM, 5 µl) and melittin inhibitor (OBAA, 5 mM, 5 µl) was added to the protocell suspension (100 µl) and incubated for 0.5 h to prevent any further lysis activity. A colony of live *E. coli* cells (OD_{600} = 5, 5 µl) was then added to the protocell suspension and incubated for 10 min to facilitate the capture of live bacteria within the cytoplasmic-like region of the bacteriogenic protocells. A solution containing a lysate—prepared by treating a single population of *P. aeruginosa* cells in buffer (20 mM Tris-HCl, 2 mM EDTA, pH 8.0) with lysozyme and melittin (final concentrations, 2 mg ml^{-1} for both, 1 h) followed by NAG3 (10 mM, 5 µl, 0.5 h) and OBAA (5 mM, 5 µl, 0.5 h)—was then added to seal the protocell membrane with lipid fragments.

Energization of the living/protocell construct was initiated by addition of glucose (1 mg ml^{-1}; LB broth (peptone (2 mg ml^{-1}) and yeast extract (1 mg ml^{-1})) to generate ATP inside the living *E. coli* guest cells and subsequently charge the host bacteriogenic protocells with ATP by extracellular secretion. An aqueous solution of rhodamine-B-labelled G-actin (final concentration, 50 µg ml^{-1}) was then added to the protocell suspension followed by a F-actin-initiator buffer (500 mM KCl, 20 mM $MgCl_2$ in 100 mM Tris, pH 7.5) to activate the self-assembly of a F-actin proto-cytoskeletal network within the bacteriogenic protocells by a self-sufficient mechanism of ATP production. ATP biogeneration within the hybrid protocells was readily sustained by replenishing the nutrients in the external medium. Nutrients were replenished in the first 3 h after incubation and then replenished every 6 h. To avoid changes in additive concentrations, we matched the concentration of all of the buffers in the post-added nutrient solutions, including the Mg^{2+}-containing actin polymerization buffer and the LB nutrient buffer, for the implanted live bacteria. Moreover, the reaction tubes were sealed to avoid water evaporation and concomitant increases in concentration.

Live-cell gene expression in bacteriogenic protocells

Bacteriogenic protocells with entrapped live *E. coli* (strain DH2) cells were prepared as described above followed by addition of 5 µl of 1,4-dithiothreitol (1 mM) and 2-mercaptoethanol (1 mM) and incubation for 1 h to inactivate the residual DNase I. Monitoring and analysis of gene expression were performed as described in the 'Endogenous gene expression in bacteriogenic protocells' and 'Protein gel electrophoresis and western blot analysis' sections above.

Luciferase assays

ATP concentrations in a pure *E. coli* colony or bacteriogenic coacervate-based PDDA/UTP protocells containing an enzyme-based ATP generation pathway or live *E. coli* cells were determined using luciferase assays. The reactions were performed in 50 mM Tris-HCl (pH 7.8) buffer with 1 µg ml^{-1} luciferase and 20 µg ml^{-1} D-luciferin. Luminescence intensities were recorded using a plate reader.

Kinase assays

For kinase activity assays, bacteriogenic protocells with entrapped live *E. coli* cells were prepared as described above. The kinase activity was then determined by a two-step cascade reaction. Peptide substrates (1 µl; Z′-LYTE Ser/Thr 5 Peptide, from Z′-LYTE Kinase Assay Kit, 0.1 mM diluted by 5× kinase buffer) were added to 200 µl of the protocell suspension and incubated for 1 h at room temperature.

Then, 5 µl of development solution (from the Z′-LYTE Kinase Assay Kit, development reagents included) was added and the mixture was incubated for a further 1 h at room temperature. Then, 5 µl of a stop reagent (from Z′-LYTE Kinase Assay Kit) was added and fluorescence intensities (excitation/emission: 400/445 nm, 520 nm) were recorded using a plate reader. Control experiments using bacteriogenic protocells without entrapped live *E. coli* cells were undertaken using the same procedures.

Assembly of membrane-coated, water-filled vacuoles in bacteriogenic protocells

A total of 40 µl from a suspension of bacteriogenic protocells was placed on an O-slide and the aqueous supernatant phase was replaced with distilled water to generate hypotonic conditions.

3D reconstruction and volume calculation of bacteriogenic protocells

All reconstruction images and relative volume profiles of single bacteriogenic protocells were obtained by importing 3D confocal fluorescence microscopy stack files to Imaris software. The reconstruction images were created by 'surface' or 'sports' simulation in Imaris, while the volume information for the objects was checked using the 'statistics'—'volume' tool.

Optical and confocal fluorescence microscopy studies

Typically, 40 µl of the suspensions was loaded into a PEGsilane-functionalized O-slide. Optical and fluorescence microscopy images were recorded on the samples using the Leica SP5 confocal microscope with an oil-immersion ×60 lens, or a wide-field microscope with a motorized stage, adaptive focus control, and the Leica DFC365FX and DFC420C colour cameras. Fluorophores were excited using specific filters with the following excitation (λ_{ex}) and emission (λ_{em}) wavelength cut-offs: FITC, λ_{ex} = 450–490 nm, cut-off 510 nm; RITC, λ_{ex} = 515–560 nm, cut-off 580 nm; Hoechst 33,342, λ_{ex} = 355–425 nm, cut-off 455 nm. Image analysis was performed using Image J.

Pegylation of coverslips

The coverslips were precleaned with 70% ethanol by sonication for 5 min and then dried immediately with nitrogen and placed in a staining jar. A mixture containing 10 ml of toluene and 200 µl of PEGsilane was added to the jar under argon. After incubation for 24 h, the slides were rinsed individually with ethanol and dried in the air.

Curve fitting

Time-dependent fluorescence plots of the capture and compartmentalization of *E. coli* or PAO1 cells were fitted using a logistic function[44],

$$I = \frac{I_s - I_0}{1 + (t/t_{1/2})^k} + I_s$$

Where I is the fluorescence intensity value (y axis); t is the time (x axis); I_s is the saturation/maximum fluorescence intensity; I_0 is the initial fluorescence intensity; $t_{1/2}$ is the t value at the midpoint of the sigmoidal curve—before $t_{1/2}$, the slope of the curve (fluorescence intensity/adsorption increasing rate) increased; after $t_{1/2}$, the slope of the curve (fluorescence intensity/adsorption increasing rate) decreased; and k is the logistic growth rate.

According to the function, fitted curves were used to determine I_s, $t_{1/2}$ and k for both *E. coli* and PAO1 cells:

For *E. coli*,

$$I = \frac{0 - 56.4}{1 + (t/22)^3} + 56.4$$

$I_s = 56.4$, $t_{1/2} = 22$, $k = 3$.

For *P. aeruginosa*,

$$I = \frac{0 - 15.3}{1 + (t/25)^3} + 15.3$$

$I_s = 15.3$, $t_{1/2} = 25$, $k = 3$.

Reporting summary

Further information on research design is available in the Nature Research Reporting Summary linked to this article.

Data availability

All data supporting the results and conclusions are available within this paper and the Supplementary Information. Source data are provided with this paper.

38. Thakur, S., Weir, B. S. & Guttman, D. S. Phytopathogen genome announcement: draft genome sequences of 62 *Pseudomonas syringae* type and pathotype strains. *Mol. Plant Microbe Interact.* **29**, 243–246 (2016).
39. Costales, M. G. et al. A designed small molecule inhibitor of a non-coding RNA sensitizes HER2 negative cancers to herceptin. *J. Am. Chem. Soc.* **141**, 2960–2974 (2019).
40. Wiechelman, K. J., Braun, R. D. & Fitzpatrick, J. D. Investigation of the bicinchoninic acid protein assay: identification of the groups responsible for color formation. *Anal. Biochem.* **175**, 231–237 (1988).
41. Drescher, H. K. et al. L-Selectin/CD62L is a key driver of non-alcoholic steatohepatitis in mice and men. *Cells* **9**, 1106 (2020).
42. Jung, Y. et al. Metabolic signature genes associated with susceptibility to pyruvate kinase, muscle type 2 gene ablation in cancer cells. *Mol. Cells* **35**, 335–341 (2013).
43. Chiu, J., March, P. E., Lee, R. & Tillett, D. Site-directed, ligase-independent mutagenesis (SLIM): a single-tube methodology approaching 100% efficiency in 4 h. *Nucleic Acids Res.* **32**, e174 (2004).
44. Berkson, J. Application of the logistic function to bio-assay. *J. Am. Stat. Assoc.* **39**, 357–365 (1944).
45. Wittrup, K. D. & Bailey, J. E. A single-cell assay of β-galactosidase activity in *Saccharomyces cerevisiae*. *Cytometry* **9**, 394–404 (1988).
46. Spoelstra, W. K., van der Sluis, E. O., Dogterom, M. & Reese, L. Nonspherical coacervate shapes in an enzyme-driven active system. *Langmuir* **36**, 1956–1964 (2020).

Acknowledgements We thank Y. Takebayashi and J. Spencer for help with bacterial cultures; H. Sun, C. Berger-Schaffitzel and E. Bragginton for help with gel electrophoresis and western blot analysis; and A. Coutable and J. L. R. Anderson for providing the plasmid pEXP5-NT/deGFP. C.X. was funded by a Marie Curie Skłodowska Postdoctoral Fellowship (8082 H2020 PROTOBAC ERC 670 837197) and the BBSRC (BB/P017320/1). N.M. and S.M. were funded by the ERC Advanced Grant Scheme (EC-2016-674 ADG 740235).

Author contributions C.X., M.L. and S.M. conceived the experiments. C.X. and N.M. performed the experiments. C.X. and M.L. undertook the data analysis. C.X., M.L. and S.M. wrote the manuscript.

Competing interests The authors declare no competing interests.

Additional information

Supplementary information The online version contains supplementary material available at https://doi.org/10.1038/s41586-022-05223-w.

Correspondence and requests for materials should be addressed to Mei Li or Stephen Mann.

Peer review information *Nature* thanks the anonymous reviewers for their contribution to the peer review of this work.

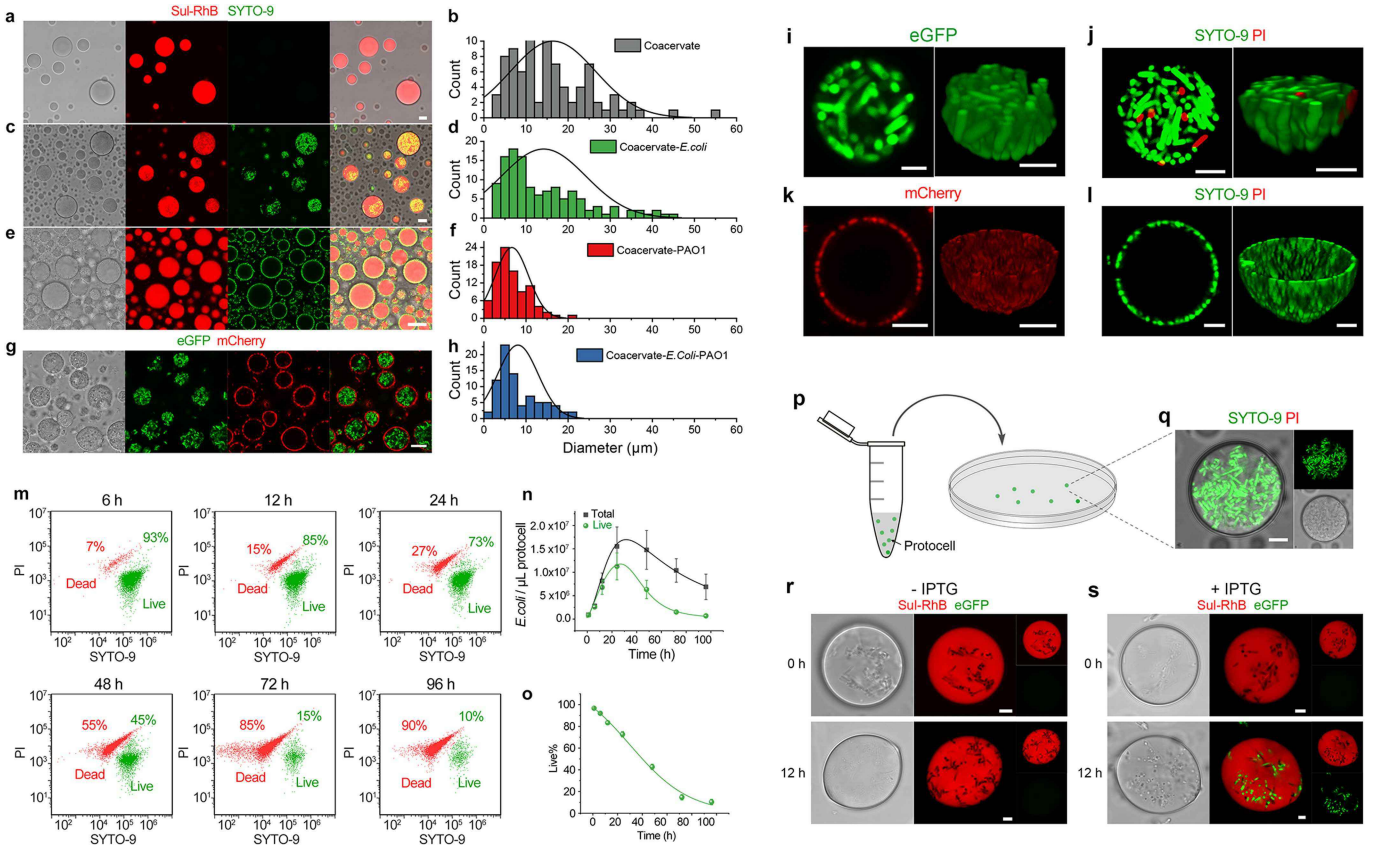

Extended Data Fig. 1 | Distribution and viability of co-captured bacterial colonies in coacervate microdroplets. a–**h**, Confocal microscopy images (**a**,**c**,**e**,**g**) and corresponding size distributions (**b**,**d**,**f**,**h**) of as-prepared PDDA/ATP coacervate droplets (Sul-RhB stained, red fluorescence) (**a**,**b**), coacervate droplets (Sul-RhB stained, red fluorescence) with captured *E. coli* cells (SYTO-9 stained, green fluorescence) (**c**,**d**), captured PAO1 cells (SYTO-9 stained, green fluorescence) (**e**,**f**), or co-captured *E. coli* (eGFP-expressed, green fluorescence) and PAO1 (mcherry-expressed, red fluorescence) cells (**g**,**h**). **i**-**l**, 2D and 3D confocal fluorescence microscopy images of single PDDA/ATP coacervate droplets after incubation with *E. coli* eGFP (**i**,**j**) or *P. aeruginosa* mCherry (**k**,**l**). Expression of eGFP (green fluorescence) or mCherry (red fluorescence) is used to locate the bacteria as dense clusters within the droplet interior (*E. coli*, **i**) or as a thin outer shell on the surface of the droplet (*P. aeruginosa*, **k**). Live and dead bacterial cells are stained with DNA dyes SYTO-9 (green, membrane permeable) and PI (red, membrane impermeable), respectively. Note the prevalence of living cells associated with both the interior and surface of the coacervate droplets. **m**–**n**, FACS 2D gated data (**m**) and time-dependent plot profiles (**n**) of live/dead *E. coli* BL21(DE3) cell population/numbers in PDDA/ATP coacervate droplets after incubation with LB broth. Green dots correspond to live bacteria (stained by SYTO-9); red dots correspond to dead bacteria (stained by PI). **o**, Plot showing time-dependent decrease in percentage of live *E. coli* cells within PDDA/ATP coacervate after incubation with LB broth. Number of experiments in **n**, **o**, n = 3; error bars, standard deviations. **p**, Graphic showing transfer of PDDA/ATP coacervate droplets containing sequestered live *E. coli* BL21(DE3) cells into a petri dish. **q**, Confocal fluorescence and brightfield microscopy images showing live (green fluorescence)/dead (red fluorescence) staining for *E. coli* BL21 (DE3) cells in a single PDDA/ATP coacervate after being transferred to a petri dish and cultured for 3 h. The bacteria remain viable within the coacervate droplets under these conditions. **r**,**s** Confocal fluorescence and brightfield microscopy images of *E. coli* Rosetta(DE3) cells with a IPTG-sensitive eGFP plasmid and sequestered within single PDDA/ATP coacervate in the absence (**r**) and presence (**s**) of IPTG. Gene expression leading to protein synthesis and folding is only observed in (**s**). All scale bars, 5 μm.

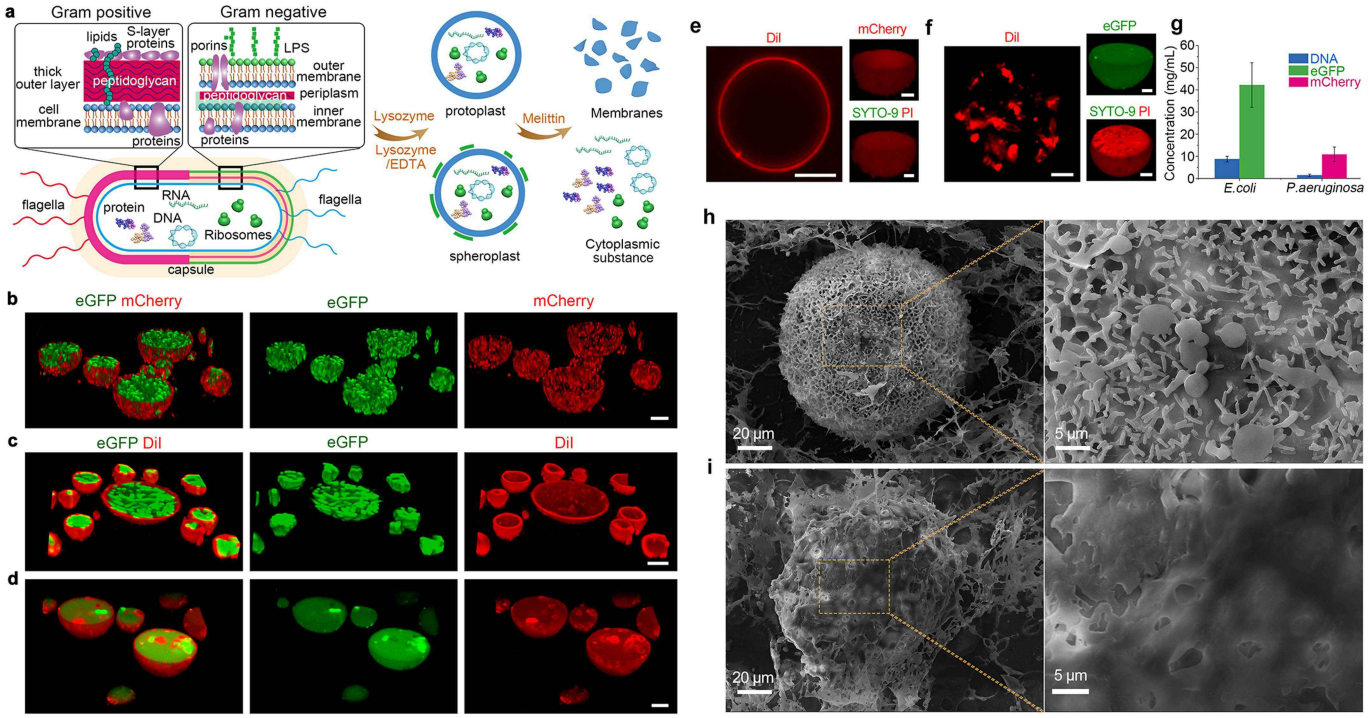

Extended Data Fig. 2 | Construction of bacteriogenic protocells by stepwise in situ lysis of co-captured bacteria populations in coacervate microdroplets. a, Schematic representation showing disassembly and release of *E. coli* and/or *P. aeruginosa* cell membrane and cytoplasmic components via a stepwise lysis procedure using lysozyme and melittin. *E. coli* and *P. aeruginosa* are gram-negative bacteria. The procedure is also applicable to gram-positive bacteria such as *S. aureus*. **b**–**d**, Confocal fluorescence microscopy images of PDDA/ATP coacervate droplets containing binary populations of *E. coli* eGFP and *P. aeruginosa* mCherry cells before lysis (**b**), after lysis of only *P. aeruginosa* mCherry (**c**), and after lysis of both bacteria (**d**). Before lysis, populations of *E. coli* and *P. aeruginosa* cells are spatially separated between the interior and surface regions of the coacervate droplets, respectively (**b**; left image, eGFP(green)/mCherry (red) overlay; centre, eGFP; right, mCherry). Lysis of the surface-adsorbed *P. aeruginosa* population results in coacervate droplets comprising a smooth and continuous shell of phospholipid bilayer membrane fragments derived from the dead *P. aeruginosa* cells (red fluorescence ring, DilC18 cytoplasmic membrane staining) along with an interior containing high numbers of live *E. coli* cells (**c**). Lysis of both bacterial populations disrupts all the cells (DilC18 staining throughout) and releases eGFP into the coacervate matrix to produce bacteriogenic protocells (**d**). All scale bars, 5 µm. **e**, Confocal fluorescence microscopy images of a single PDDA/ATP coacervate droplet recorded after capture of *E. coli* cells and treatment with lysozyme and melittin. Lysis of the *E. coli* cells releases membrane components (left, DilC18 lipid staining, red fluorescent aggregates), expressed proteins (upper right, eGFP, green fluorescence) and DNA (lower right, SYTO-9/PI staining, red fluorescence) into the coacervate interior. All scale bars, 5 µm. **f**, As for (**e**) but for captured and lysed PAO1 cells. Membrane fragments are redistributed around the droplet surface to produce a continuous outer shell (left, DilC18 lipid staining, red fluorescence), and release of low levels of expressed proteins (upper right, m-Cherry, red fluorescence) and DNA (lower right, SYTO-9/PI staining, red fluorescence) into the coacervate matrix. All scale bars, 5 µm. **g**, Concentrations of eGFP (green column), mCherry (red column) and DNA (blue column) in a population of coacervate droplets after complete lysis of captured *E. coli*-eGFP or PAO1-mCherry cells. Numbers of samples for tests: n = 3. **h**, **i**. Low (left) and high (right) magnification scanning electron micrographs of freeze dried single PDDA/ATP coacervate droplets before (**h**) and after (**i**) lysis of captured *E. coli* and PAO1 cells; the bacteriogenic protocell produced after disassembly of the surface attached PAO1 cells is enclosed by a shell of disordered cytomembrane fragments.

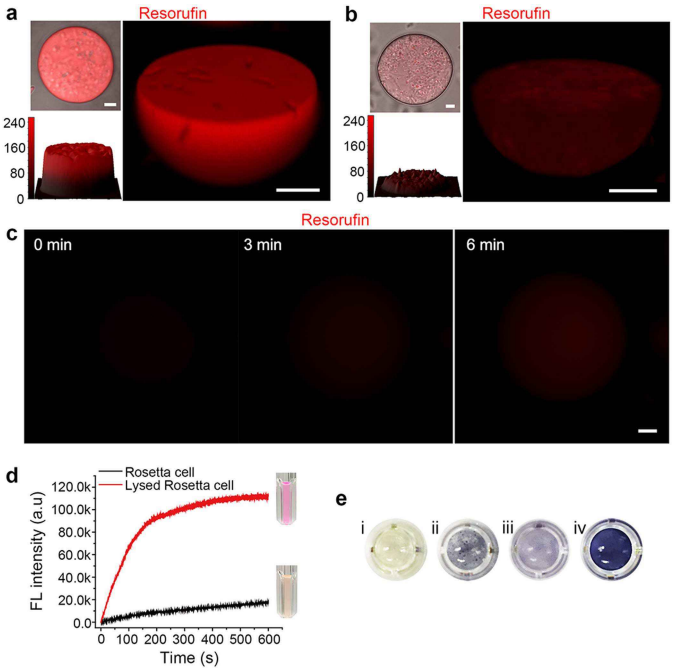

Extended Data Fig. 3 | Enzyme activity (β-gal) and glycolysis in bacteriogenic protocells. a,**b**, 3D (right) and 2D (left) confocal fluorescence microscopy images of a single bacteriogenic protocell (**a**) and single coacervate droplet with co-captured non-lysed bacteria (**b**) 10 min after addition of RBG. β-gal activity is observed only after lysis and construction of the protocells. Typically, the final red fluorescence intensity of the bacteriogenic protocells was about 10 times higher than that of the non-lysed bacteria-loaded droplets. β-gal activity arises from the lysis of *E. coli* Rosetta (strain DE3) cells, which along with PAO1 cells were used for protocell construction in place of the non-β-gal-active *E. coli* strain BL21. **c**, Time-dependent fluorescence microscopy images of a single coacervate droplet with co-captured *E. coli* Rosetta (strain DE3) and PAO1 cells after addition of RBG showing no apparent β-galactosidase-mediated production and sequestration of resorufin (red fluorescence). The absence of enzyme activity arises from the cell membrane impermeability of RBG. **d**, Time-dependent fluorescence profiles of RBG reactions with *E. coli* Rosetta cells (black line) or lysed *E. coli* Rosetta cells (red line). Ex: 560 nm, Em: 594 nm. The absence of enzyme activity arises from the cell membrane impermeability of RBG[45]. **e**, Photographs of the sample well holder containing various samples after 30 min exposure to LB broth and assayed for glycolysis via conversion of pyruvate to L-lactate and formation of the reduced purple dye formazan; native coacervate droplets (i), bacteriogenic protocells (ii), bacterial lysate (iii), *E. coli* cells and PAO1 (2: 1; OD = 1, iv). Lysate and protocells were generated from the same bacterial concentrations as used in the cell sample. All scale bars, 5 µm.

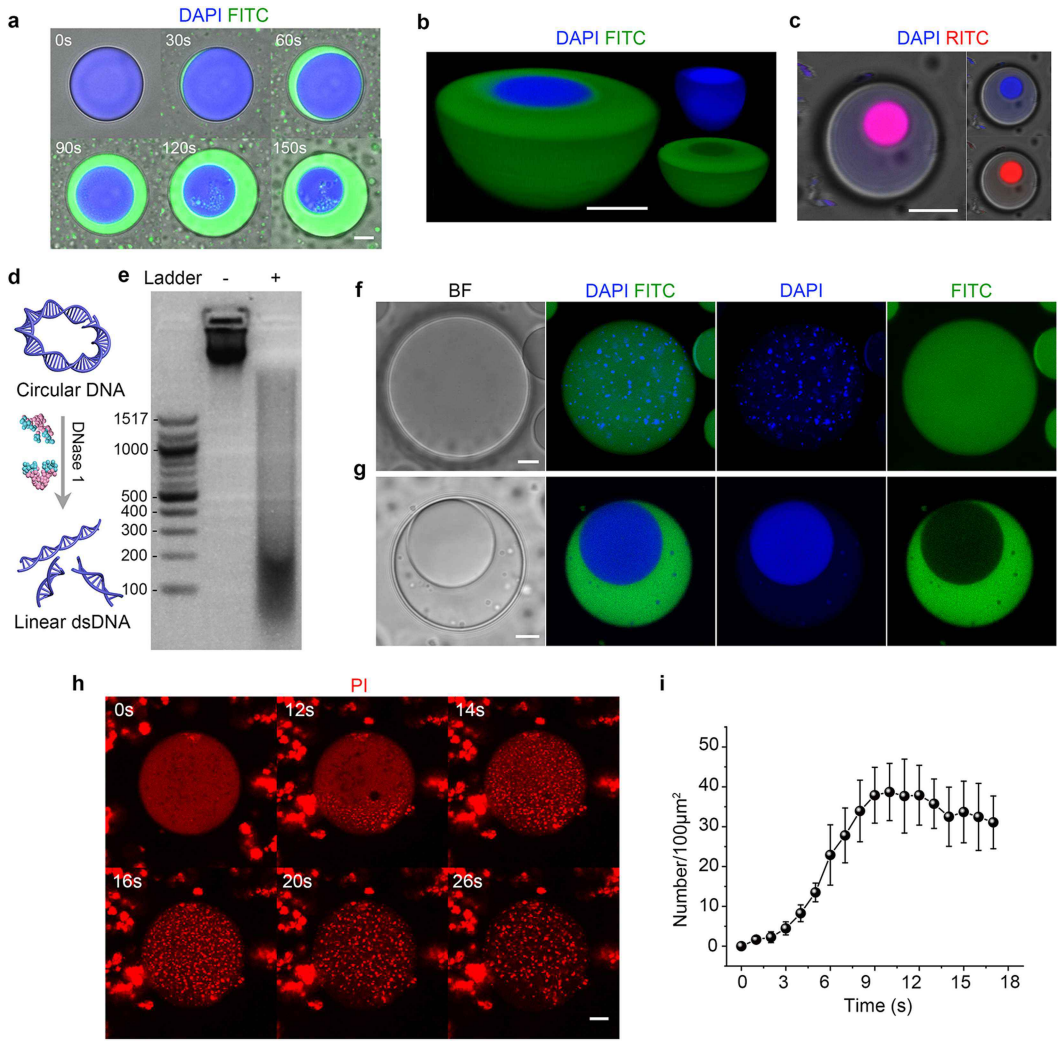

Extended Data Fig. 4 | In situ condensation and spatial localization of bacterial DNA within bacteriogenic protocells. a, Time-dependent series of confocal microscopy images showing liquid-liquid phase separation and formation of a single DNA-enriched droplet in a PDDA/ATP/histone/DNA coacervate micro-droplet after addition of FITC-CM-dextran (70 kDa). DNA and CM-dextran are labelled with DAPI (blue fluorescence) and FITC (green fluorescence), respectively. CM-dextran is excluded from the DNA-enriched sub-compartment. **b**, 3D confocal fluorescence microscopy images of a single PDDA/ATP/histone/DNA (wt ratio; 3.2: 5: 2: 1) coacervate droplet after addition of FITC-CM-dextran (70 kDa, green fluorescence). Filtered and overlay images are shown. **c**, Confocal microscopy images of multiphase coacervate droplets showing co-location of DNA (blue fluorescence) and histone (red fluorescence) in the phase-separated sub-compartment. Samples were prepared using mixtures of PDDA/ATP/RITC-histone/DAPI-DNA. Images were recorded 10 min after addition of FITC-CM-dextran (70 kDa). **d**, Illustration showing cleavage of circular (plasmid) DNA by DNase I to produce linear dsDNA fragments with blunt ends. **e**, DNA electrophoresis profiles for commercial purified *E. coli* DNA before (–) and after (+) incubation with DNase I for 30 min in the presence of aqueous $MnCl_2$. Oligonucleotides with molecular weights less than 200bp are produced. **f**,**g**, Confocal bright field (BF) and fluorescence microscopy images of PDDA/ATP/histone/*E. coli* plasmid DNA coacervate droplets after addition of FITC-CM-dextran (70 kDa, green fluorescence) without (**f**) or with (**g**) subsequent treatment with DNase1 to produce linear fragments. Phase separation of the circular or linear DNA produces, respectively, sub-micrometre-sized discontinuous aggregates (**f**) or a single demixed sub-compartment (**g**) (blue fluorescence, DAPI-stained DNA). One possibility is that differences in histone-DNA binding for the circular and linear variants influences the surface tension of the phase-separated nuclei and their ability to undergo coalescence. **h**, Time-dependent series of confocal fluorescence microscopy images of a single bacteriogenic protocell before and after addition of CM-dextran showing nucleation of a population of plasmid DNA/histone condensates (red fluorescence) throughout the molecularly crowded interior. The protocells were prepared from histone-containing PDDA/ATP coacervate droplets followed by *in situ* lysis of co-captured *E. coli* and PAO1 cells to release the bacterial DNA *in situ*. DNA is stained with PI. **i**, Plot showing time-dependent increase in the number of DNA/histone particles nucleated within individual bacteriogenic protocells after addition of CM-dextran at $t = 0$. Data normalized to protocell cross-sectional area (number/100 μm^2) to account for different protocell sizes. Typically, single protocells would contain around 200 particles of the DNA/histone condensates, which remain dispersed in the protocell interior with minimal aggregation. Number of protocells measured, n = 4; errors bars, standard deviations. All scale bars, 5 μm.

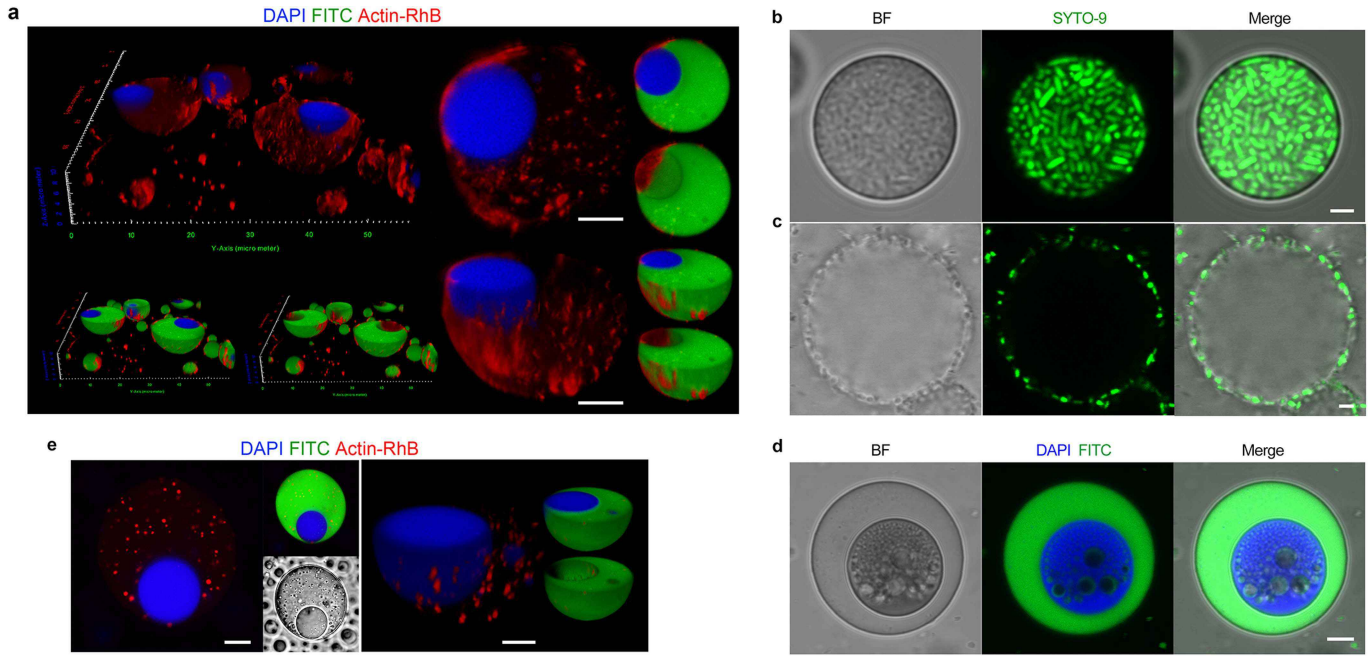

Extended Data Fig. 5 | Actin assembly in PDDA/ATP or PDDA/UTP coacervate-based bacteriogenic protocells. a, 3D confocal fluorescence microscopy images showing *in situ* assembly of short RhB-labelled actin filaments (red fluorescence) in PDDA/ATP coacervate-based bacteriogenic protocells comprising a bacterial DNA-derived phase-separated histone-containing sub-compartment (proto-nucleus, blue fluorescence, (DAPI stained) embedded in a coacervate matrix (proto-cytoplasm, green fluorescence (FITC-CM-dextran)). Low (left side) and high (right side) magnification images of multiple or single protocells are shown. Uptake of RhB-G-actin from the external solution via diffusion through the protocell membrane (not stained) results in ATP-mediated polymerization to produce fibre-like aggregates specifically in the proto-cytoplasm, but not in the proto-nucleus. Fibre growth was inhibited due to the high concentration of ATP (*ca*. 200 mM) present in the coacervate phase. **b**–**d**. Confocal bright field (BF) and fluorescence microscopy images of single PDDA/UTP coacervate droplets after capture of *E. coli* (**b**) or *P. aeruginosa* (**c**) cells in the droplet interior or at the surface, respectively. In both cases, the prevalence of live bacteria is shown by SYTO-9 staining of DNA (green fluorescence). **d**, Single PDDA/UTP/histone/DNA coacervate droplet after addition of FITC-CM-dextran (green fluorescence) showing formation of a phase separated DNA/histone-enriched sub-compartment (DAPI stained, blue fluorescence). **e**, 2D (left) and 3D (right) confocal fluorescence microscopy images showing the distribution of actin (red fluorescence, RhB-labelled) in a single PDDA/UTP coacervate-based bacteriogenic protocell containing a phase-separated DNA/histone sub-compartment (blue fluorescence, (DAPI stained) dispersed in a FITC-CM-dextran-enriched coacervate matrix (green fluorescence). No ATP-generating system is present. As a consequence, actin-rich aggregates, 0.1–1 µm in size (red spots) in place of F- actin filaments are observed. All scale bars, 5 µm.

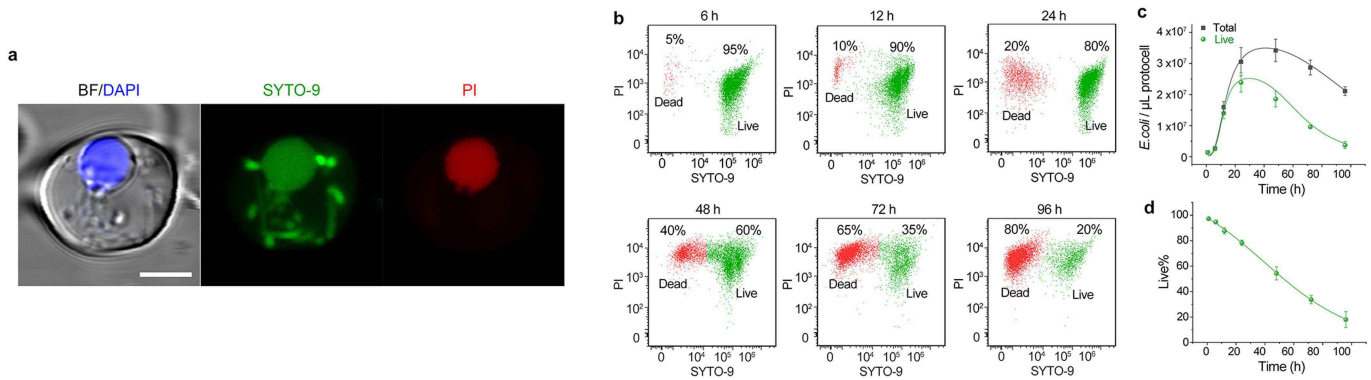

Extended Data Fig. 6 | Viability of implanted *E. coli* cells in PDDA/UTP coacervate-based bacteriogenic protocells. a, Confocal fluorescence microscopy images showing live/dead stain for *E. coli* BL21 (DE3) cells in a single PDDA/UTP coacervate-based bacteriogenic protocell with a single proto-nucleus (blue/red fluorescence, DAPI/PI stained). To inactivate the lysozyme and melittin inside the protocell and in the solution, the protocells were pre-incubated with lysozyme inhibitor NAG3 and melittin inhibitor OBAA for 0.5 h before adding of *E. coli*. The live *E. coli* cells were stained by SYTO-9 (green fluorescence), which can penetrate live bacteria, and dead cells were stained by PI (red fluorescence), which can only penetrate dead bacteria and can also stain the DNA in the proto-nucleus. Images showed that almost all of the *E. coli* cells remained alive in the protocells after 3 h. Scale bar, 5 μm. **b**,**c**, FACS 2D gated data (**b**) and time-dependent plot profiles (**c**) of live/dead *E. coli* cell population/numbers in bacteriogenic protocells after incubation with LB broth. Green dots correspond to live bacteria (stained by SYTO-9); red dots correspond to dead bacteria (stained by PI). **d**, Plot showing time-dependent decrease in percentage of live *E. coli* cells within bacteriogenic protocells after incubation with LB broth.

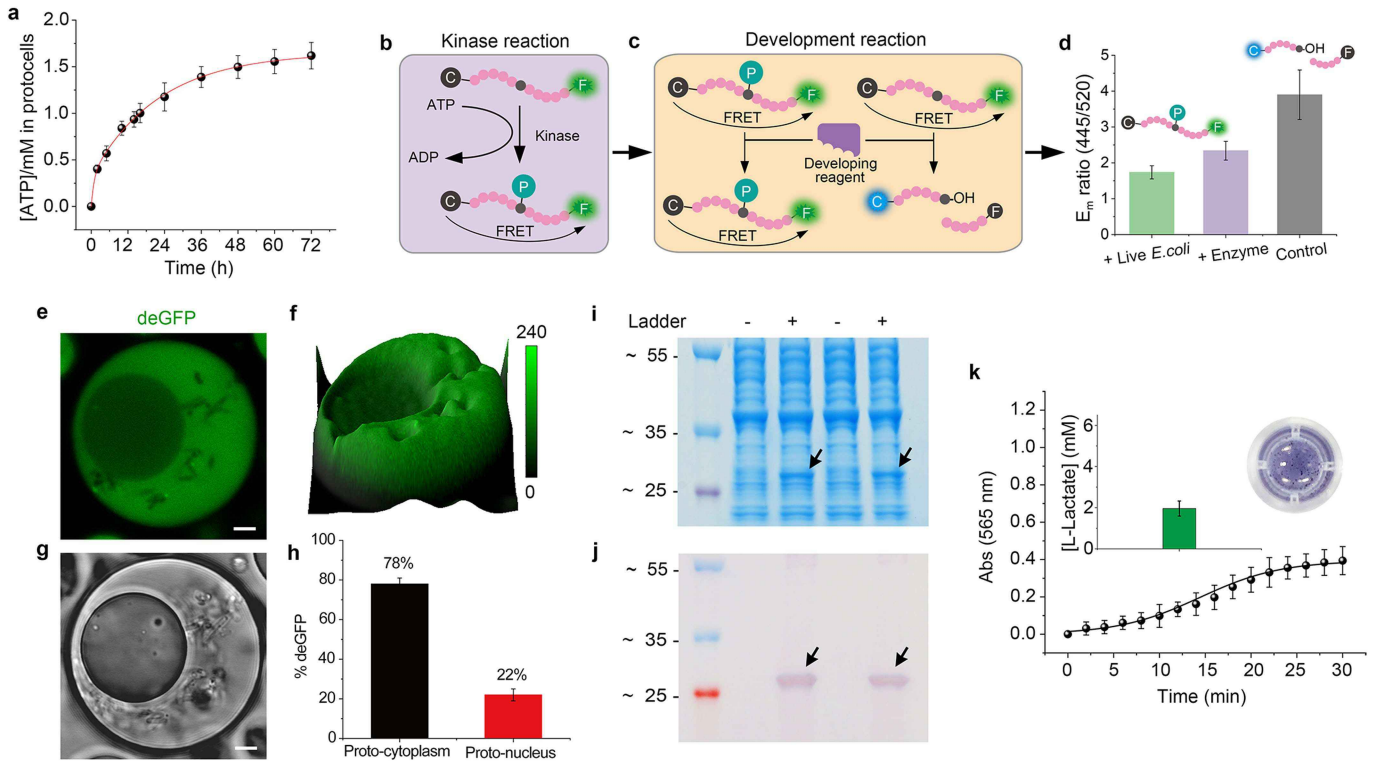

Extended Data Fig. 7 | Enhanced cytomimetic properties of bacteriogenic protocells energized by implanted live *E. coli* cells. a, Time-dependent plots of ATP concentrations produced in bacteriogenic protocells via endogenous bio-generation (entrapped live *E. coli* cells) over a period of 72 h. The bacterial ATP profiles were dependent on the nutrient levels in the experimental system. Number of samples, n = 3; error bars are standard deviations. **b**, **c**, Schematic diagram of the Z′-LYTE biochemical assay for kinase activity detection in protocells. The Z′-LYTE biochemical assay employs a FRET-based, coupled-enzyme format and is based on the differential sensitivity of phosphorylated and non-phosphorylated peptides to proteolytic cleavage. The pentapeptide substrate is labelled with two fluorophores, coumarin (C) and fluorescein (F) −one at each end−that make up a FRET pair. In the primary reaction (**b**, the kinase reaction), the kinase transfers the γ-phosphate of ATP to a single serine or threonine residue in the synthetic peptide substrate. In the secondary reaction (**c**, the Development reaction), a site-specific protease (the Development reagent) recognizes and cleaves non-phosphorylated peptides. Phosphorylated peptides exhibit suppressed cleavage by the Development reagent. Cleavage disrupts FRET between the donor (coumarin) and acceptor (fluorescein) fluorophores on the peptide, whereas uncleaved phosphorylated peptides maintain FRET. A ratiometric method, which calculates the ratio (the Emission Ratio = Coumarin Emission (445 nm)/Fluorescein Emission (520 nm) of donor emission to acceptor emission after excitation of the donor fluorophore at 400 nm, quantitates reaction progress. **d**, The emission ratio (445/520) of protocells with endogenous ATP bio-generation (entrapped live *E. coli* cells (+), green column, 1.7), with endogenous ATP chemical (enzyme) generation (PK/PEP/ADP pathway, purple column, 2.3) or ATP present in the released bacterial lysate (no live E. coli, grey column, 3.9) after incubation with Z′-LYTE biochemical substrate reagents and developing reagent for 1 h under room temperature. Number of samples, n = 3; error bars are standard deviations. **e**–**j**, In vitro translation and transcription in live *E. coli*-containing bacteriogenic protocells (PDDA/UTP); Confocal fluorescence (**e**) and bright field (**g**) microscopy image, 3D fluorescence surface plot (**f**) and weight percent (%) and of deGFP partitioning (**h**) in the cytoplasm- and nucleus-like regions in a single hybrid protocell. Scale bars, 5 μm. Gel electrophoresis profiles (**i**) and western blotting images (**j**) of extracted proteins obtained after salt-induced disassembly of protocells with (+) or without (−) plasmid pEXP5-NT/deGFP. Arrow in (**i**, **j**) shows additional band at 27 kDa that was absent without the plasmid and which stains on exposure to an anti-GFP antibody (chicken) and goat anti-chicken IgY H&L (alkaline phosphatase). **k**, Glycolysis in ATP-generating *E. coli*-containing bacteriogenic protocells (PDDA/UTP); time-dependent plot of changes in absorption at 565 nm, final concentration of L-lactate produced (insert, left) and photograph of sample after 30 min (insert, right) associated with endogenous ATP biogeneration. Number of samples, n = 3; error bars are standard deviations. For comparison with protocells containing only released bacterial lysate; see Fig. 3h–j in the main manuscript.

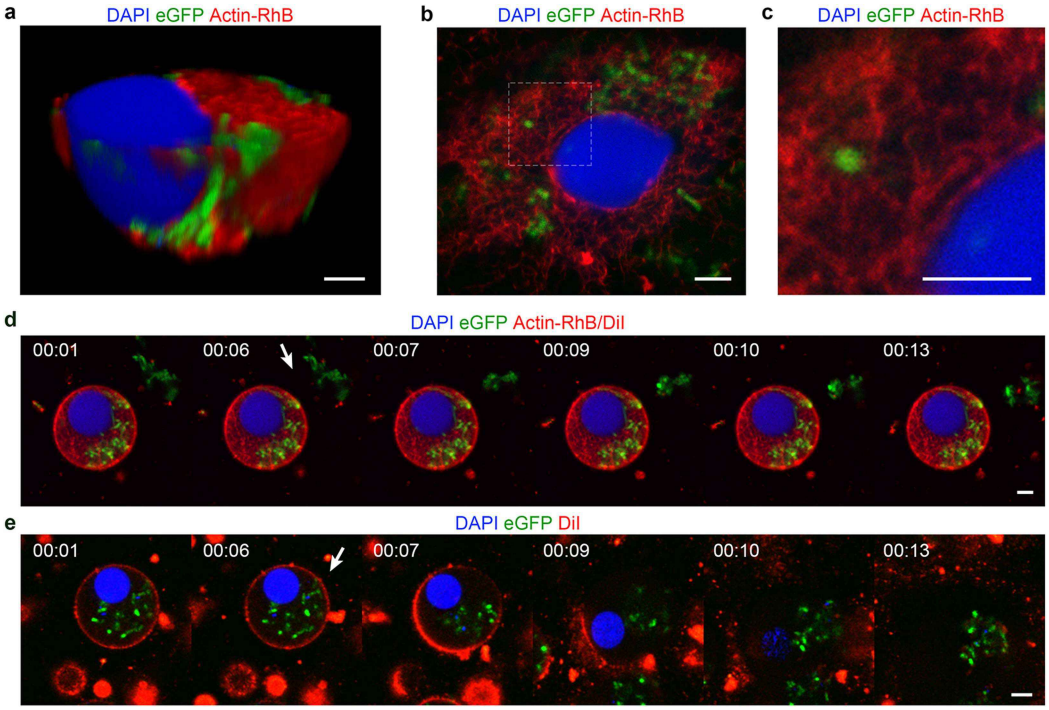

Extended Data Fig. 8 | F-actin-mediated structural stability of living/synthetic cell constructs. a, 3D confocal fluorescence microscopy images of an individual living/synthetic cell construct showing extensive network of F-actin micro-filaments (red fluorescence, RhB-labelled actin) within the cytoplasmic-like space of a bacteriogenic host protocell. The DNA/histone sub-compartment (blue fluorescence, DAPI, DNA stain) and guest *E. coli* eGFP cells (green fluorescence, expressed GFP) are immobilized within the cytoskeletal-like matrix. Continuous on-site bio-production of ATP from a glucose source and uptake of G-actin give rise to extensive hydrogelation of the protocell interior. Images are recorded 0.5 h after addition of G-actin. **b**,**c**, Confocal fluorescence microscopy images recorded at low (**b**) and high (**c**) magnification of a single bacteriogenic protocell with entrapped live *E. coli* cells showing extensive cytoskeletal-like network (red fluorescence, RhB-F-actin filaments) within the cytoplasmic-like space of the bacteriogenic host protocell. The DNA/histone proto-nucleus (blue fluorescence, DAPI DNA stain) and guest *E. coli* eGFP cells (green fluorescence, expressed GFP) are immobilized within the cytoskeletal-like matrix. Images recorded 2 days after completion of internal hydrogelation. The enlarged image shown in **c** is taken from the dashed box shown in **b**. **d**,**e**. Confocal fluorescence microscopy of bacteriogenic hybrid protocell with (**d**) and without (**e**) F-actin after exposure to 200 mM NaCl (added at $t = 6$ s (white arrows)). Outer membrane (red fluorescence, DiI stain; PAO1-derived lipids), molecularly crowded proto-cytoplasm (non-fluorescent), proto-cytoskeleton (red fluorescence), membrane-free DNA/histone proto-nucleus (blue fluorescence). The protocells with F-actin (**d**) showing minimal shrinking under hypertonic conditions, while without F-actin, the protocells are disassembled. All scale bars, 5 µm.

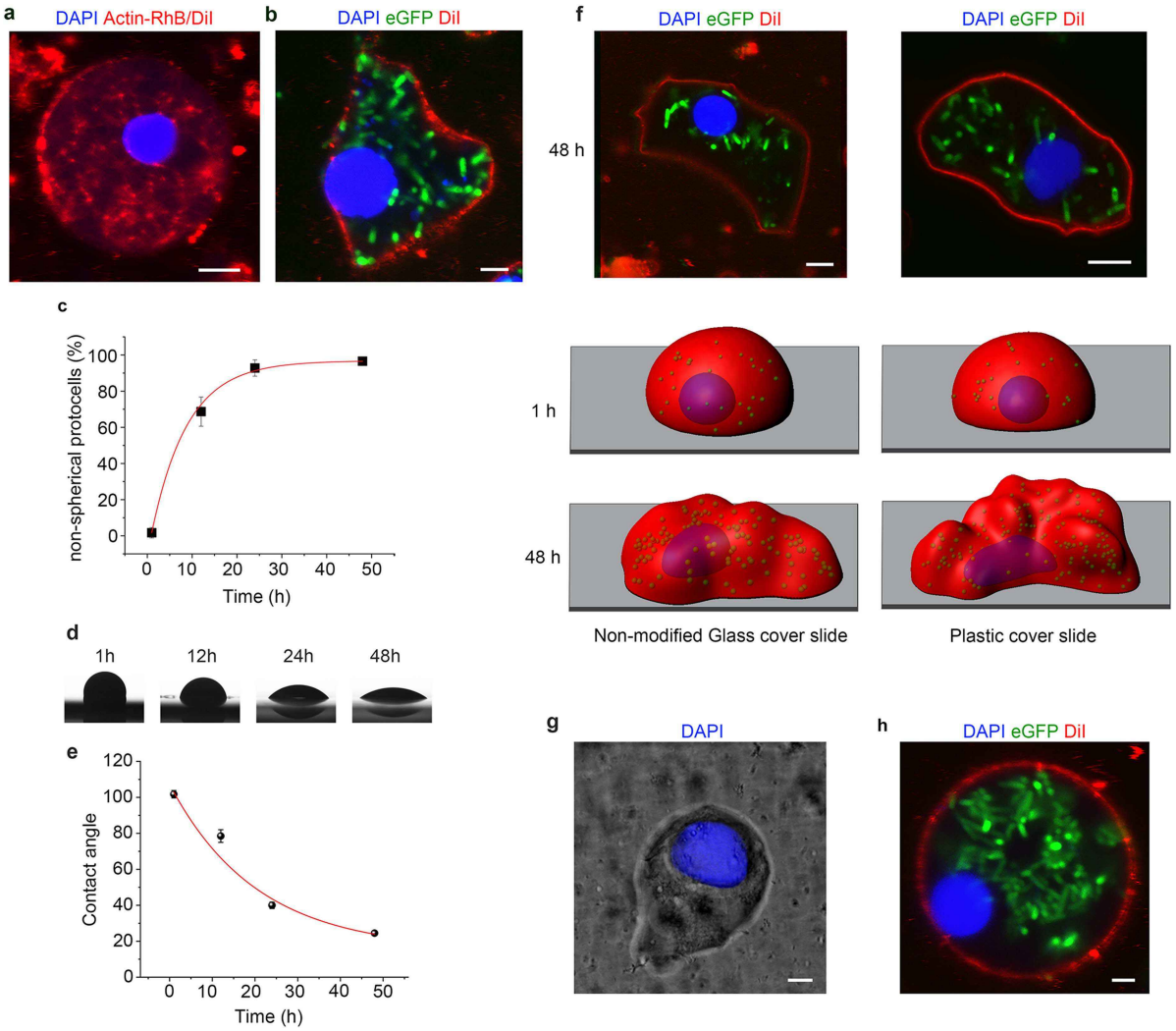

Extended Data Fig. 9 | Mechanism of live cell-mediated morphogenesis in bacteriogenic protocells. a, Confocal fluorescence microscopy image of an individual bacteriogenic protocell with F-actin and endogenous ATP chemical (enzyme) generation (PK/PEP/ADP pathway) after incubation with substrates (PEP/ADP) for 1 day showing no morphological change associated with F-actin or ATP production. **b**, Confocal fluorescence microscopy image of an individual amoeba-like bacteriogenic protocell with entrapped *E. coli* eGFP cells after incubation with LB broth for 1 day. Scale bars, 5 µm. **c**, Percentage of protocells with non-spherical morphologies using a circularity analysis[46]. Number of samples, n = 3; error bars, standard deviations. **d**,**e** Optical images (**d**) and contact angle plot (**e**) showing time-dependent increase in wettability and decrease in contact angle for single droplets of a concentrated suspension of living/synthetic constructs mounted on a pegylated glass slide. **f**, 2D Confocal fluorescence microscopy images (top) and 3D Imaris reconstruction images (bottom) of bacteriogenic protocells with entrapped *E. coli* eGFP cells showing progressive formation of amoeba-like living/synthetic microscale constructs with retention of internal organization and outer membrane after incubation on a non-modified glass cover slide or plastic cover slide. Data recorded at 1 h and 48 h. Staining: DNA/histone condensate (DAPI, blue); guest live *E. coli* cells (eGFP, green dots); outer membrane (DilC18, red). Scale bars, 10 µm. **g**, Confocal microscopy image (left) of an individual bacteriogenic protocell containing entrapped *E. coli* cells and F-actin after incubation with LB broth for 48 h; the image was recorded in aqueous suspension, DNA staining by DAPI, blue fluorescence, scale bar, 10 µm. **h**, Confocal fluorescence microscopy image of an individual bacteriogenic protocell with high levels of entrapped *E. coli* eGFP cells after incubation with LB broth for 1 h. The *E. coli*-eGFP cells were washed with PBS buffer to remove bacterial secretions before addition to the protocells. Scale bar, 5 µm.

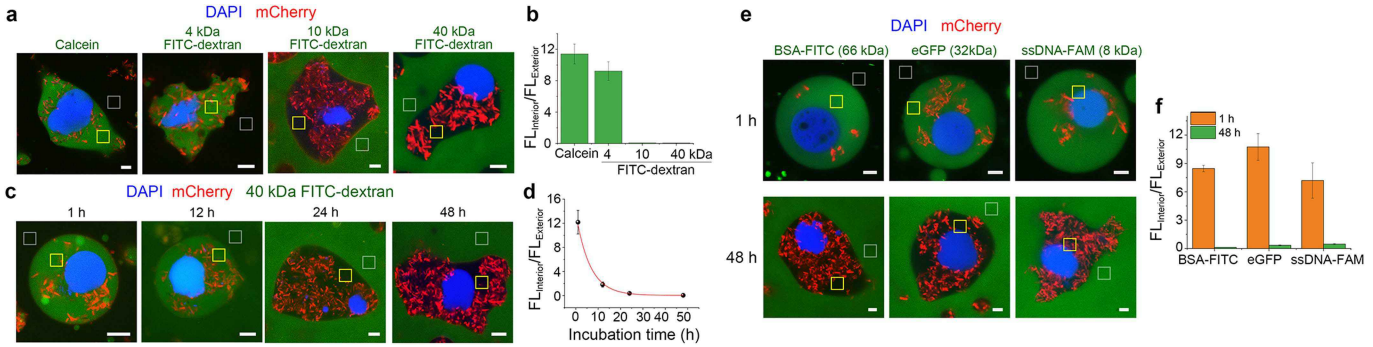

Extended Data Fig. 10 | Time-dependent decrease in membrane permeability of living/synthetic constructs. a-d, Confocal fluorescence microscopy images of single living/synthetic constructs incubated for 48 h followed by addition of various green-fluorescent solutes to the external phase (**a**), and corresponding uptake ratios (grey-value ratios, $FL_{interior}/FL_{exterior}$) (**b**), showing impermeability of 10 and 40 kDa FITC-dextran. **c**, as for (**a**) but after different periods of biological activity followed by addition of 40 kDa dextran. **d**, Corresponding uptake ratios determined for different incubation times shown in (**c**); **e**,**f** Confocal fluorescence microscopy images (**e**) and corresponding uptake ratios (grey-value ratios, $FL_{interior}/FL_{exterior}$) (**f**) of single living/synthetic constructs incubated for 1h and 48 h followed by addition of various green-fluorescent solutes (FITC-BSA, Mw = 66 kDa), eGFP (32 kDa) and ssDNA-FAM (8 Da) to the external phase. All scale bars, 5 µm.

nature portfolio

Corresponding author(s): Prof. Stephen Mann FRS
Dr. Mei Li

Last updated by author(s): Jul 13, 2022

Reporting Summary

Nature Portfolio wishes to improve the reproducibility of the work that we publish. This form provides structure for consistency and transparency in reporting. For further information on Nature Portfolio policies, see our Editorial Policies and the Editorial Policy Checklist.

Statistics

For all statistical analyses, confirm that the following items are present in the figure legend, table legend, main text, or Methods section.

n/a	Confirmed
☐	☒ The exact sample size (*n*) for each experimental group/condition, given as a discrete number and unit of measurement
☐	☒ A statement on whether measurements were taken from distinct samples or whether the same sample was measured repeatedly
☒	☐ The statistical test(s) used AND whether they are one- or two-sided *Only common tests should be described solely by name; describe more complex techniques in the Methods section.*
☒	☐ A description of all covariates tested
☒	☐ A description of any assumptions or corrections, such as tests of normality and adjustment for multiple comparisons
☐	☒ A full description of the statistical parameters including central tendency (e.g. means) or other basic estimates (e.g. regression coefficient) AND variation (e.g. standard deviation) or associated estimates of uncertainty (e.g. confidence intervals)
☒	☐ For null hypothesis testing, the test statistic (e.g. *F*, *t*, *r*) with confidence intervals, effect sizes, degrees of freedom and *P* value noted *Give P values as exact values whenever suitable.*
☒	☐ For Bayesian analysis, information on the choice of priors and Markov chain Monte Carlo settings
☒	☐ For hierarchical and complex designs, identification of the appropriate level for tests and full reporting of outcomes
☒	☐ Estimates of effect sizes (e.g. Cohen's *d*, Pearson's *r*), indicating how they were calculated

Our web collection on statistics for biologists contains articles on many of the points above.

Software and code

Policy information about availability of computer code

Data collection	Microscope image collections were performed by Leica DFC365FX and Leica DFC420C; Flow Cytometry experiments were carried on a BD LSRFortessa™ X-20 cell analyzer; Scanning electron microscopy (SEM) were taken on a Jeol IT300 SEM instrument; Proteomics data were acquired using the Orbitrap Fusion Tribrid mass spectrometer
Data analysis	Microscope image data analysis was performed by Fiji Image J and Icy; 3D reconstruction of microscope images was performed by Imaris; Flow Cytometry data was analyzed by FlowJo V10; Proteomics data were processed and quantified using Proteome Discoverer software v2.1 ; All data plots and histograms were performed by Origin 8.

For manuscripts utilizing custom algorithms or software that are central to the research but not yet described in published literature, software must be made available to editors and reviewers. We strongly encourage code deposition in a community repository (e.g. GitHub). See the Nature Portfolio guidelines for submitting code & software for further information.

Data

Policy information about availability of data

All manuscripts must include a data availability statement. This statement should provide the following information, where applicable:

- Accession codes, unique identifiers, or web links for publicly available datasets
- A description of any restrictions on data availability
- For clinical datasets or third party data, please ensure that the statement adheres to our policy

All data generated or analyzed during this study are included in this published article (and its supplementary information files). Source data are provided with this paper.

Field-specific reporting

Please select the one below that is the best fit for your research. If you are not sure, read the appropriate sections before making your selection.

☒ Life sciences ☐ Behavioural & social sciences ☐ Ecological, evolutionary & environmental sciences

For a reference copy of the document with all sections, see nature.com/documents/nr-reporting-summary-flat.pdf

Life sciences study design

All studies must disclose on these points even when the disclosure is negative.

Sample size	All experiments were conducted with bacterial cell lines with multiple available biological replicates and based on previous experience with specific experimental setup. No statistical measures were used to predetermine sample size. We typically performed at least 3 biological replicates for each experiment, unless otherwise noted in the figure legends.
Data exclusions	No data was excluded from analysis in this study
Replication	All experiments were reliably reproduced as stated in the text, and detailed methods provided to aid in their replication by others.
Randomization	Randomization was not relevant to this study.
Blinding	Blinding was not relevant to this study.

Reporting for specific materials, systems and methods

We require information from authors about some types of materials, experimental systems and methods used in many studies. Here, indicate whether each material, system or method listed is relevant to your study. If you are not sure if a list item applies to your research, read the appropriate section before selecting a response.

Materials & experimental systems

n/a	Involved in the study
☐	☒ Antibodies
☒	☐ Eukaryotic cell lines
☒	☐ Palaeontology and archaeology
☒	☐ Animals and other organisms
☒	☐ Human research participants
☒	☐ Clinical data
☒	☐ Dual use research of concern

Methods

n/a	Involved in the study
☒	☐ ChIP-seq
☐	☒ Flow cytometry
☒	☐ MRI-based neuroimaging

Antibodies

Antibodies used	1. Chicken polyclonal to GFP, anti-GFP antibody, Abcam, Cat# ab13970 2. Goat Anti-Chicken IgY H&L (Alkaline Phosphatase) Abcam, Cat# ab6878
Validation	1. https://www.abcam.com/gfp-antibody-ab13970.html 2. https://www.abcam.com/goat-chicken-igy-hl-alkaline-phosphatase-ab6878.html

Flow Cytometry

Plots

Confirm that:

☒ The axis labels state the marker and fluorochrome used (e.g. CD4-FITC).

☒ The axis scales are clearly visible. Include numbers along axes only for bottom left plot of group (a 'group' is an analysis of identical markers).

☒ All plots are contour plots with outliers or pseudocolor plots.

☒ A numerical value for number of cells or percentage (with statistics) is provided.

Methodology

Sample preparation	200 µL of a coacervate or coacervate droplet suspension was added to the Flow Cytometry tube, and 2 µL of a single strain of bacteria or mixture of bacterial strains (E.coli Rosetta™(DE3), P. aeruginosa PAO1, initial OD = 20, final OD = 0.2 OD), or a bacterial lysate were added. The samples were shaked sufficiently before taking everytime before taking the Flow Cytometry tests.
Instrument	BD LSRFortessa™ X-20 cell analyzer
Software	FlowJo V10 software
Cell population abundance	Cell sorting not employed.
Gating strategy	We applied forward and side scatter parameter (FSC>300, SSC>0) to exclude debris. The fraction of cells was then quantified using indicated gates (contour plot).

☐ Tick this box to confirm that a figure exemplifying the gating strategy is provided in the Supplementary Information.